



Zero-dimensional Predictive Hydrogen Combustion Model

Mitra Malekpour

Thesis for the degree of Master of Science in Engineering
Division of Combustion Engines
Department of Energy Sciences
Faculty of Engineering | Lund University

Zero-dimensional Predictive Hydrogen Combustion Model

Mitra Malekpour

February 2023, Lund

This project for the degree of Master of Science in Engineering has been conducted at the Division of Combustion Engines, Department of Energy Sciences, Faculty of Engineering, Lund University.

Supervisor at the Department of Energy Sciences was Professor Öivind Andersson.

Supervisor at Volvo Technology Group was Ulf Aronsson.

Examiner at Lund University was Sebastian Verhelst.

The project was carried out in cooperation with Volvo Technology Group.

Thesis for the Degree of Master of Science in Engineering

ISRN LUTMDN/TMHP-23/5512-SE

ISSN 0282-1990

© Mitra Malekpour 2023

Division of Combustion Engines

Department of Energy Sciences

Faculty of Engineering, Lund University

www.energy.lth.se

MASTER THESIS

Zero-dimensional Predictive Hydrogen Combustion Model

Mitra Malekpour

mi5345ma-s@student.lu.se

Supervisor: Öivind Andersson

oivind.andersson@energy.lth.se

Industrial supervisor: Ulf Aronsson

ulf.aronsson@volvo.com

VOLVO GROUP

January 2023

Abstract

Due to the emissions of carbon dioxide and other greenhouse gases discharged from cars and trucks, and their negative impact on the environment and climate, many interests have been shifted into exploring the usage of alternative fuels. One of these alternative fuels is hydrogen which exhibits favourable properties such as not producing any carbon emissions.

In this thesis project, a zero-dimensional three-zone predictive model for hydrogen combustion in a spark ignited internal combustion engine is developed. In this model, the combustion chamber has been divided into three zones, an unburned zone, a burned zone, and a flame front zone. The model incorporates a flame geometry model, an entrainment model, and the fundamentals of thermodynamics together with a laminar and turbulent flame speed model. The flame geometry model computes a flame volume, which in turn is used in the entrainment model to give an approximation of the entrained mass. The laminar and turbulent flame speed model provides an estimation of how fast the flame is propagating inside the combustion chamber.

The conducted simulations in form of parameter sweeps of engine speed, inlet and exhaust pressures, and inlet temperature show reasonable trends. Validation and calibration of the model with experimental data will be done in future works.

Sammanfattning

På grund av utsläppen av koldioxid och andra växthusgaser från bilar och lastbilar och deras negativa påverkan på miljö och klimat, har många intressen flyttats till att utforska användningen av alternativa bränslen. En av dessa alternativa bränslen är väte som uppvisar gynnsamma egenskaper då det inte har något koldioxidutsläpp.

I detta examensarbete utvecklas en noll-dimensionell, trezons prediktiv modell för vätgasförbränning i en gnisttänd förbränningsmotor. I denna modell har förbränningskammaren delats upp i tre zoner, en oförbränd zon, en bränd zon och en flamfrontszon. Modellen innehåller en flamgeometrimodell, en entrainment-modell och en laminär och turbulent flamhastighetsmodell. Flamgeometrimodellen beräknar en flamvolym, som i sin tur används i entrainment-modellen för att ge en approximation av den totala massan på gasen i flammen. Den laminära och turbulenta flamhastighetsmodellen ger en uppskattning av hur snabbt flammen fortplantar sig.

De genomförda simuleringarna i form av parametersvep av motorvarvtal, inlopps- och avgasttryck samt inloppstemperatur visar rimliga trender. Validering och kalibrering av modellen med experimentella data kommer att genomföras i framtida arbeten.

Acknowledgements

First and foremost, I would like to thank Volvo Trucks Technology for giving me the opportunity to carry out my master thesis project with them. It has been a couple of amazing and valuable months, working with such a brilliant, competent, and helpful group of people and being able to ask for their guidance at any time.

Special thank you and deepest gratitude to Ulf Aronsson, my industrial supervisor at Volvo, for his ceaseless patience and mentorship throughout this project. It has been an honor to have you as my supervisor and to be able to work so closely with you. Thank you for sharing your experience and expertise with me and for always being one step ahead when facing problems.

I also would like to thank Öivind Andersson, my supervisor at the Department of Energy Sciences, for his guidance during this time. Thank you for providing a constant assistance and for always staying positive.

This master thesis project is the final step of my education in Mechanical Engineering at Lund University, and being able to accomplish this would have not been possible without help of so many people. One of these people is Ingrid Holmberg, who has always patiently listened to me in the most difficult times during my education and come up with solutions.

Last, but not least, the most special gratitude to my wonderful parents and my lovely partner. Without your unconditional love, support, and motivation I would not be here today.

Abbreviations

ICE	Internal Combustion Engine
ICES	Volvo's Internal Combustion Engine Simulation Program
AFR	Air-fuel Ratio
AFS	Stoichiometric Air-fuel Ratio
TKE	Turbulent Kinetic Energy
TI	Turbulent Intensity
FBR	Fraction Burned Residual Gases
BR	Burnt Ratio
RPM	Revolutions Per Minute
RPS	Revolutions Per Second
DI	Direct Injection
LPDI	Low Pressure Direct Injection
HPDI	High Pressure Direct Injection
PFI	Port Fuel Injected
PFI	Port Fuel Injected

Contents

Abstract

Sammanfattning

Acknowledgements

Abbreviations

1	Introduction	1
1.1	Limitations	2
2	Theory	3
2.1	Hydrogen properties	3
2.2	Zero-dimensional models	3
2.3	Governing equations	4
2.4	Fuel injection systems	8
2.5	In-cylinder geometry	9
2.6	Chemical kinetics	10
2.7	Cantera	11
2.8	ICES: Volvo's Internal Combustion Engine Simulation program	11
3	Methodology	13
3.1	Combustion model	13
3.2	Flame geometry	15
3.3	Laminar flame speed	17
3.4	Implementation and setup in ICES	19
4	Results	22
4.1	Laminar flame speed	22
4.2	Implementation in ICES	35
5	Discussion	44
6	Conclusion	46

Bibliography

Appendix

List of Figures

1	Cylinder geometry	10
2	Flame geometry when $r_{flame} \leq \frac{bore}{2}$	16
3	Flame geometry when $r_{flame} > \frac{bore}{2}$	17
4	ICES GUI	20
5	ICES inlet and exhaust valve lifts	21
6	Laminar flame speed as a function of equivalence ratio, ϕ	22
7	Laminar flame speed dependency on temperature and ϕ at 1 bar	23
8	Laminar flame speed dependency on pressure and ϕ at 298 K	23
9	Method 1: Result for fitting $S_{L,ref}$ using equation 44	24
10	Method 1: Result for fitting $S_{L,ref}$ using equation 49	24
11	Method 1: The temperature fit	25
12	Method 1: The pressure fit	26
13	Method 1: Laminar flame speed evaluation at the reference conditions	27
14	Method 1: Laminar flame speed evaluation at conditions differing from the initial conditions	28
15	Method 1: Laminar flame speed evaluation at conditions differing from the initial conditions	29
16	Method 1: Observed vs predicted laminar flame speed	30
17	Method 2: Observed vs predicted laminar flame speed (training data contain 100 data points)	31
18	Method 2: Observed vs predicted laminar flame speed (training data contain 900 data points)	32
19	Method 2: Observed vs predicted laminar flame speed (evaluation of validation data)	33
20	Method 2: Laminar flame speed at higher temperatures at $\phi = 0.5$	34
21	Method 2: Laminar flame speed at higher temperatures at $\phi = 0.25$	35
22	Observed vs predicted volume: Results of regression model	36
23	Observed vs predicted volume: Results of radial basis	37
24	Observed vs predicted radius: Results of radial basis	37
25	Observed vs predicted radius: Results of the iterative solution	38
26	Comparison between flame volume from Fortran vs MATLAB	39
27	Engine Speed Sweep	40
28	Inlet Temperature Sweep	42
29	Inlet and Exhaust pressure Sweep	43

List of Tables

1	Description of the terms in laminar flame speed equation (equation 8, 9 and 10).	6
2	Description of the parameters in the entrainment model	8
3	Engine specifications	13
4	Comparison between the laminar flame speed in Cantera and experimental data found in literature	22
5	Values of the coefficients C_1-C_3 , T_1-T_5 , P_1-P_5 , and D_1-D_8	32

1 Introduction

Alternative energy sources are constantly being investigated as the threat posed by climate change continues to grow. The transportation sector's contribution to global greenhouse gas emissions is still one of the largest [1]. The emissions primarily come from burning fossil fuels. Therefore, it is of major interest to search for alternative energy carriers to minimize the environmental impact.

The possibility of using hydrogen as an alternative fuel in an internal combustion engine, ICE, or in fuel cell applications, has been explored for a long time. In fact, hydrogen was first used to power an ICE back in 1806 [2], and since then many scientists and engineers have spent time on studying the properties of hydrogen as a fuel in an ICE.

One of the most promising properties of hydrogen compared to other fuels is that it does not contain any carbon content. Consequently, carbon-based emissions such as CO and CO₂ are not produced from hydrogen combustion. The most harmful emission from hydrogen combustion in air is NO_x, which can be kept low through control of combustion conditions [3]. Leakage of unburned hydrogen may be problematic due to the risk of external combustion, especially if the vehicle is parked indoor e.g. in a garage or in a ship.

Furthermore, hydrogen exhibits a broad range of flammability, 4-74 % concentration in air, which is considerably higher compared to fuels such as gasoline or methane [4]. This allows effective engine operations for lean mixtures [5].

Hydrogen has a high autoignition temperature, at 853 K. This together with an octane number of more than 130 indicates that hydrogen should be more resistant to knocking, compared to hydrocarbon fuels [6]. However, knocking is one of the frequent constraints in hydrogen engines which limits the performance of the engine [6].

There are various drawbacks and challenges when using hydrogen in an ICE which need further investigation. The primary challenge in the development of hydrogen engines is pre-ignition. Pre-ignition occurs when the fuel mixture is ignited prior to the ignition caused by the spark plug due to e.g. hotspots in the combustion chamber. The reason behind this abnormal combustion behavior is the wide flammability range, low ignition energy of hydrogen and high speed of flame propagation [6]. Pre-ignition affects the efficiency of engine operation and results in damages to the engine.

There are certainly several advantages with hydrogen-fueled ICEs, but at the same time there are many challenges and uncertainties about the nature of hydrogen combustion. To be able to eliminate these uncertainties, it is desirable to model the combustion process of hydrogen. In this way, the combustion process can be simulated under various engine conditions and for various air-fuel relations. Consequently, diverse issues can be addressed and investigated, and solutions to these issues can be suggested. Thus, this thesis project aims to build a zero-dimensional model for hydrogen combustion in a spark-ignition ICE with help of fundamental thermodynamic relations.

Due to the complex nature of the engine processes, it is of great importance to clearly define the objectives of the model. These objectives need to match

the level of detail and complexity in the model. Combustion processes can be modelled in great detail with help of e.g. CFD, computational fluid dynamics. However, three-dimensional CFD models are typically used in single cycle simulations with fixed boundary conditions. For hardware selection in engine development, there is a large demand for fast zero-dimensional models in gas exchange simulations. In these models, spatial resolution is sacrificed but instead high calculation speed is obtained.

For the purpose of this thesis project, a zero-dimensional, three-zone model is developed in MATLAB to analyze the in-cylinder pressure, temperature, and the rate of heat release. The project is performed in collaboration with Volvo Trucks Technology and the model, after completion in MATLAB, is implemented in ICES, Volvo's inhouse simulation program. The results will help Volvo to develop hydrogen-fueled internal combustion engines.

The model is developed to calculate the amount of unburned gas burning at each time step or as a function of the crank angle. With other words, the author has modelled the heat release rate as a function of the crank angle.

1.1 Limitations

The project timeline is 20 weeks of work corresponding to 30 credits, which applies a time limitation on the project.

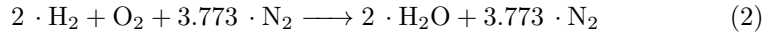
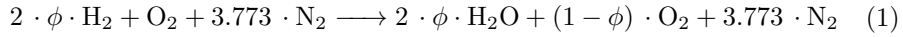
The software used in this project are MATLAB, Spyder for python programming, Microsoft Visual Studio for Fortran programming, GT-Power by Gamma Technologies, and ICES. Currently, it is not possible to run physical tests at the company's laboratory. Therefore, the primary focus of this project has been on modelling.

The abnormal combustion behavior such as knocking and pre-ignition have not been investigated in this project. In addition, looking into turbulence in detail for hydrogen combustion is left out in this project. The developed combustion model has been prepared to take in an existing turbulent kinetic energy model as an input and use it to calculate a turbulent flame speed.

2 Theory

2.1 Hydrogen properties

Combustion of hydrogen in air has the general form expressed in equation 1. In this equation, ϕ is the fuel-air equivalence ratio, and this equation is valid for $\phi \leq 1$. Equation 1 can be simplified into equation 2 by assuming stoichiometric conditions, i.e. $\phi = 1$.



For hydrogen, the stoichiometric AFR, air-fuel ratio, is 34.1499 and calculated according to equation 3. The stoichiometric AFR can be shortened to *AFS*.

$$AFR_{stoichiometric} = AFS = \frac{m_{air}}{m_{fuel}} = \frac{m_{oxygen} + 3.773 \cdot m_{nitrogen}}{m_{hydrogen}} \Rightarrow \quad (3)$$

$$AFS = \frac{2 \cdot 15.999 + 3.773 \cdot 2 \cdot 14.0067}{2 \cdot 2 \cdot 1.008} = 34.1499$$

The equivalence ratio for a given mixture can be expressed as air-fuel equivalence ratio, λ , which is the ratio of actual AFR to *AFS*. Moreover, ϕ , fuel-air equivalence ratio, is also used to indicate a mixture's equivalence ratio. ϕ and λ follow a simple relation according to

$$\lambda = \frac{AFR}{AFS} = \frac{1}{\phi} \quad (4)$$

2.2 Zero-dimensional models

Zero-dimensional models are fast and simple models that do not have any spatial/dimensional resolution [7]. This means that there is no information provided to describe flow physics in detail or to determine the certain position where the highest turbulence occurs in the combustion chamber. Zero-dimensional models rely on average values of certain quantities [8]. In these models, the content of the combustion chamber can be distributed into a single-zone, two zones, three zones or multi zones, which are described briefly in the following sections.

2.2.1 Single-zone models

In [9], a zero-dimensional single-zone engine model has been developed, where the content of the cylinder is assumed as one thermodynamic system and distributed into one single imaginary zone. Afterwards, the ideal gas law and the law of conservation of energy are applied to this single zone to determine combustion behavior.

2.2.2 Two-zone models

Two-zone modelling approach is used in [10]. The combustion chamber has been divided into two zones, an unburned zone and a burned zone, which are separated from each other by the flame front. The fresh air-fuel mixture exists in the unburned zone and the combustion products are in the burned zone. The flame front is where the chemical reactions take place. It is a thin boundary layer and its movement depends on the flame propagation speed.

2.2.3 Three-zone models

A three-zone combustion model has been developed in [11], where an unburned zone, a burned zone and a flame front zone coexist in the combustion chamber. The mixture that has not yet burned exists in the unburned zone, and as the combustion process continues, this unburned mixture gradually flows into the flame front zone. In the flame front zone, the specific proportion of the mixture burns, which releases heat and consequently causes the temperature to increase. Afterwards, this proportion flows into the burned zone. The unburned zone becomes smaller and smaller after each time step until it finally vanishes, meaning that the combustion is finished.

The three-zone modelling approach is similar to the method in two-zone modelling. The difference is that, in a two-zone model a proportion of the unburned mixture in the unburned zone burns immediately and moves into the burned zone. However, in the three-zone model the same proportion of the unburned mixture moves first into the flame front zone. The model then considers the fact that this unburned proportion requires a specific amount of time to burn. When this time has passed, the unburned proportion is burned and flows to the burned zone.

2.2.4 Multi-zone models

In [8], the combustion model is a multi-zone model. A multi-zone model is based on creating a new, separate combustion zone in each time step during the whole combustion process.

2.3 Governing equations

2.3.1 Ideal gas law

The gas species inside a combustion chamber can be treated as ideal gases and follow the ideal gas law stated in equation 5.

$$P_{incyl} \cdot V = m_{incyl} \cdot R \cdot T \quad (5)$$

2.3.2 Specific heat capacity

Specific heat capacity at constant pressure has the general form according to equation 6. In this equation, Q is the amount of energy/heat required for a temperature rise ΔT for a specific quantity of hydrogen, m_{H_2} . Q can additionally be expressed with help of the lower heating value, Q_{LHV} , according to equation 7.

$$(c_{p,avg})_{mixture} = \frac{Q}{m_{H_2} \cdot \Delta T} \quad (6)$$

The lower heating value for hydrogen is $120 \frac{MJ}{kg}$ [12], which is defined as the amount of available thermal energy that is released by combusting a specific quantity of the fuel.

$$Q = Q_{LHV} \cdot m_{H_2} \quad (7)$$

2.3.3 Laminar flame speed

Laminar flame speed is the speed at which a steady, planar, one-dimensional, and stretch-free flame propagates relative to the unburned gas mixture ahead of it [13] [14]. It is an important property of a flammable mixture which depends on pressure, temperature, mixture equivalence ratio, and diluent concentration. Laminar flame speed affects the combustion rate, e.i. the burning rate, in an spark ignition engine.

The laminar flame speed is calculated according to equation 8 and the complete explanation for each term of the equation is given in table 1 [15]. In this equation, $S_{L,ref}$, α , and β are constants for a specified fuel and a specified equivalence ratio. These constants are known for fuels such as propane, isooctane, and methanol but the author could not find the values of these constants for hydrogen in the literature. The $S_{L,ref}$ term is calculated according to equation 9 [15]. The dilution effect, $f(dilution)$, is an addition to the original laminar flame speed equation in [15] according to [16] and [17].

$$S_L = S_{L,ref} \cdot \left(\frac{T_{un}}{T_{ref}} \right)^\alpha \cdot \left(\frac{P_{incyl}}{P_{ref}} \right)^\beta \cdot f(dilution) \quad (8)$$

$$S_{L,ref} = B_m + B_\phi \cdot (\phi - \phi_m)^2 \quad (9)$$

$$f(dilution) = 1 - 0.75 \cdot DEM \cdot (1 - (1 - 0.75 \cdot DEM \cdot dilution)^7) \quad (10)$$

Because B_m , B_ϕ , and ϕ_m in $S_{L,ref}$, α , and β are all constants unknown for hydrogen and dependent on a specific equivalence ratio ϕ , they can be expressed according to equations 11-13 respectively. To be able to calculate laminar flame speed for a hydrogen-air mixture of a specified equivalence ratio at a known temperature and pressure, constants C_1 - C_3 , T_1 - T_5 , and P_1 - P_5 need to be known.

$$S_{L,ref} = C_1 + C_2 \cdot (\phi - C_3)^2 \quad (11)$$

$$\alpha = T_1 + T_2 \cdot \phi + T_3 \cdot \phi^2 + T_4 \cdot \phi^3 + T_5 \cdot \phi^4 \quad (12)$$

Parameter	Description
S_L	Laminar flame speed [$\frac{m}{s}$]
$S_{L,ref}$	Laminar flame speed at reference temperature and pressure [$\frac{m}{s}$]
B_m	Maximum laminar speed [$\frac{m}{s}$]
B_ϕ	Laminar speed roll-off value [$\frac{m}{s}$]
ϕ_m	Equivalence ratio corresponding to maximum laminar flame speed
T_{un}	Temperature of the unburned gas [K]
T_{ref}	Reference temperature = 298 K
α	Temperature exponent
P_{incyl}	Pressure inside the cylinder [Pa]
P_{ref}	Reference pressure = 101325 Pa
β	Pressure exponent
$f(dilution)$	Dilution effect
DEM	Dilution effect multiplier
dilution	Dilution

Table 1: Description of the terms in laminar flame speed equation (equation 8, 9 and 10).

$$\beta = P_1 + P_2 \cdot \phi + P_3 \cdot \phi^2 + P_4 \cdot \phi^3 + P_5 \cdot \phi^4 \quad (13)$$

Considering chemical equation 2 and the molar masses of different species in this equation, the mass of the air and the products can be calculated according to equations 14 and 15. In these equations n is the number of moles of a specie and M is the molar mass of that specie.

$$m_{air} = (n \cdot M)_{N_2} + (n \cdot M)_{O_2} \quad (14)$$

$$m_{products} = (n \cdot M)_{H_2O} + (n \cdot M)_{N_2} \quad (15)$$

Dilution is defined as fraction burned residual gases, FBR , present in the unburned zone according to

$$dilution = \frac{FBR \cdot m_{air}}{m_{air} + m_{products}} \quad (16)$$

2.3.4 Turbulent kinetic energy and turbulent intensity

Turbulent kinetic energy, TKE , is defined according to equation 17, where u'_x , u'_y , and u'_z are turbulent velocity components [18]. Assuming that the turbulent velocity components are equal in the x , y , and z direction, equation 17 can be simplified to equation 18.

$$TKE = \frac{1}{2} \cdot (\overline{(u'_x)^2} + \overline{(u'_y)^2} + \overline{(u'_z)^2}) \quad (17)$$

$$TKE = \frac{3}{2} \cdot \overline{(u')^2} \quad (18)$$

Turbulent intensity, TI , is related to u' according to equation 19 [19]. Equations 18 and 19 together, give the correlation between TKE and TI , which can be expressed according to equation 20.

$$(TI)^2 = 3 \cdot \overline{(u')^2} \quad (19)$$

$$TI = \sqrt{2 \cdot TKE} \quad (20)$$

2.3.5 Turbulent flame speed

Turbulent flame speed can be calculated according to equation 21 with help of laminar flame speed and turbulent intensity [19]. C and n in this equation can be treated as calibration parameters.

$$S_T = S_L \cdot \left(1 + C \cdot \left(\frac{TI}{S_L} \right)^n \right) \quad (21)$$

An alternative expression has been provided by [20] to calculate turbulent flame speed, which is given in equation 22. In this equation, C_{TFS} and C_{FKG} are calibration constants used to adjust the effect of turbulent intensity and the initial growth rate of the flame kernel. L_i is the integral length scale, which is a constant parameter, and is additionally used when computing the entrained mass in the next subsection. The term $\frac{r_{flame}}{L_i}$ in this equation indicates that the impact of turbulence is smaller in the beginning of the combustion when the radius of the flame is small.

$$S_T = S_L + C_{TFS} \cdot TI \cdot \left(1 - \frac{1}{1 + C_{FKG} \cdot \left(\frac{r_{flame}}{L_i} \right)^2} \right) \quad (22)$$

Both these methods have been implemented in ICES and it is possible for the user to choose the desired one for the simulation. It is important to keep in mind that there are other correlations for S_T that can be used to calculate the turbulent flame speed which might work better for hydrogen combustion.

2.3.6 Entrained and burned masses under turbulent condition

The main role of turbulence is to wrinkle the flame, leading to an increase in the surface area of the flame and consequently the interface area between the unburned and burned zones. This increases the rate at which burnt gas is produced and results in a flame brush thickness, which can be mathematically captured with help of the entrainment model.

The entrainment model is a mathematical way of capturing the S-shaped curve of the mass fraction burned. In this model, two different masses need to be taken into account, an entrained mass and a burned mass. The entrained mass is the mass of the unburned gas that flows from the unburned zone to the flame front region. The unburned gas do not burn immediately and require a certain

amount of time, τ , to burn [11]. The burned mass is the mass flowing from the flame front region to the burned zone as soon as it burns. These two masses can be expressed according to equations 23 and 24 [20] [21]. $\frac{dV_{flame}}{dt}$ in this equation is a measure for how much the flame volume is growing in each time step.

$$\frac{dM_e}{dt} = \rho_{un} \cdot \frac{dV_{flame}}{dt} \quad (23)$$

$$\frac{dM_b}{dt} = \frac{M_e - M_b}{\tau} \quad (24)$$

The time constant τ is calculated according to equation 25 and depends on λ , Taylor microscale length, and the laminar flame speed. λ in this equation can be computed with help of L_i , integral length scale, turbulent Reynolds number, Re_t , and a calibration constant according to equation 26 [20].

$$\tau = \frac{\lambda}{S_L} \quad (25)$$

$$\lambda = \frac{C \cdot L_i}{\sqrt{Re_t}} \quad (26)$$

Furthermore, the turbulent Reynolds number, Re_t , is computed according to 27. In table 2 a list of all the parameters in equations 23-27 with their names is given.

$$Re_t = \frac{\rho_{un} \cdot TI \cdot L_i}{\mu_{un}} \quad (27)$$

Parameter	Description
M_e	Entrained mass
ρ_{un}	Density of the unburned zone
S_L	Laminar flame speed
M_b	Burned mass
τ	Time constant
λ	Taylor microscale length
L_i	Integral length scale
Re_t	Turbulent Reynolds number
TI	Turbulent intensity
μ_{un}	Viscosity of the unburned zone

Table 2: Description of the parameters in the entrainment model

2.4 Fuel injection systems

In direct injection, DI , the fuel is directly inserted into the combustion chamber by an injector. By doing this, the fuel can mix with the air prior to ignition by spark plug and create a combustible fuel-air mixture. Direct injection can be

done in two different ways, *LPDI*, low pressure direct injection, and *HPDI*, high pressure direct injection.

Port fuel injection, *PFI*, follow the same idea of injecting the fuel, but the injection's location is different from in *DI*. In *PFI*, the fuel is injected into the intake port of the engine.

In this project, the idea is to inject the fuel prior to spark ignition to get the fuel-air mixture ready to combust and for this purpose *LPDI* has been chosen. This has not been modelled by the author and was already available in ICES.

2.5 In-cylinder geometry

Position of the piston as a function of crank angle can be expressed according to equation 28, where a , l , and θ can be seen in figure 1. Knowing the position of the piston and the compression volume, the height of the combustion chamber, the squish height, can be calculated according to equation 29. This calculation is based on the assumption that the clearance volume, V_c , is a cylindrical continuation of the cylinder upwards. V_c additionally includes the corners above the piston rings and the areas around the valves in the cylinder head.

$$y(\theta) = l + a \cdot (1 - \cos \theta) - \sqrt{l^2 - a^2 \cdot \sin^2 \theta} \quad (28)$$

$$\text{squish height} = y(\theta) + \frac{V_c}{\pi \cdot \frac{\text{bore}^2}{4}} \quad (29)$$

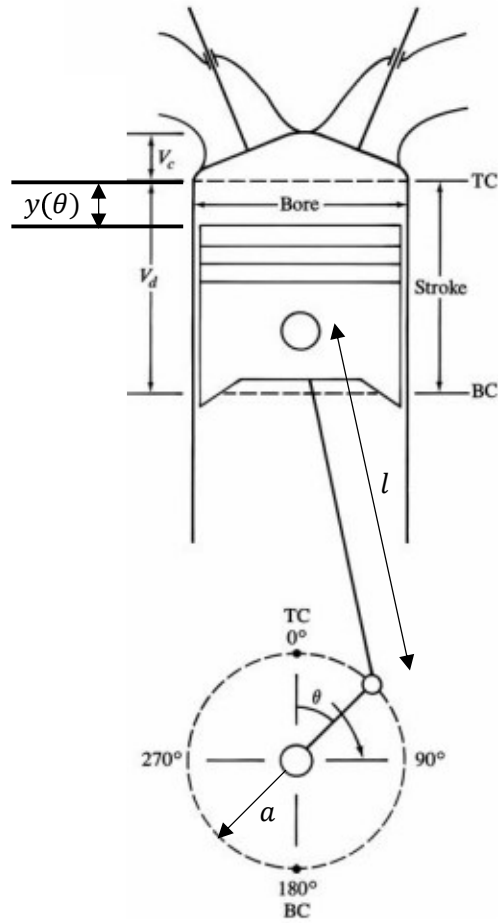


Figure 1: Cylinder geometry

The instantaneous volume of the combustion chamber as a function of the crank angle θ is given in equation 39. This volume obviously depends on the position of the piston at the specific crank angle.

$$V(\theta) = V_c + \frac{\pi \cdot bore^2}{4} \cdot y(\theta) \quad (30)$$

2.6 Chemical kinetics

Chemical kinetics is an area within chemistry that describes chemical reactions in detail. For instance, the chemical reaction in equation 2 in section 2.1 is a global reaction, which is in fact a combination of several hundred reactions. These reactions together determine how fast the global reaction occurs given different conditions such as pressure, temperature, etc. Modelling these reaction mechanisms helps understanding the combustion chemistry under the engine

conditions in an ICE. This kind of model can even explain how ignition and extinction take place considering different engine conditions.

A detailed chemical-kinetics mechanism for hydrogen combustion in air has been used in this project, which involves 57 species and 268 reactions. This mechanism has been provided by the *UC San Diego* University and used in CHEMKIN format (see Appendix) [22]. The reason behind the chosen mechanism is that it is one of the most complete and detailed mechanisms available for hydrogen combustion. However, there are other chemical-kinetics mechanisms available that have been validated at engine conditions. Choosing one of these mechanisms can lead to improvements in the laminar flame speed model, as mentioned later in chapter 5.

2.7 Cantera

Cantera is an open-source toolbox which can be used through different interfaces such as Python and MATLAB or through applications written in *C*, *C++*, and FORTRAN90 [23]. It allows the user to be able to include thermodynamics, transport models and chemical kinetics into the calculations in an efficient way. This toolbox is used in many fields such as combustion, fuel cells, batteries, detonations, etc.

2.8 ICES: Volvo's Internal Combustion Engine Simulation program

ICES is a simulation program developed by Volvo for four-stroke gasoline and diesel engines. This program together with its GUI is used for modelling and simulating engines. However, any thermodynamic system with built-in functions can be modelled and simulated in this program. A Fortran compiler, is used to be able to link the built-in functions and routines to ICES.

It is preferable by Volvo to use ICES instead of other software such as GT-Power because it allows them to run as many simulations as desired without any limitation or license issues. At the same time, using ICES provides the possibility to have full control over the development of the model and not be limited to what is offered by GT-Power.

There is currently no predictive combustion model available for hydrogen in ICES. However, a combustion model based on an empirical combustion function called Wiebe function has been implemented for hydrogen in the program. A Wiebe function is a zero-dimensional combustion model that has been extensively used in engine development, specifically for spark-ignition applications [24]. Instead of constructing a theoretical combustion model that demands large number of calculations, the Wiebe function offers a rather simple way to specify the mass fraction burned during the combustion process.

As mentioned earlier throughout chapter 1, MATLAB is used for testing the implementation of the hydrogen combustion model in the beginning of the project. Afterwards, the model is implemented in ICES and can be used for simulation. The reason behind implementation in MATLAB prior to ICES implementation is that MATLAB is more suitable for debugging, which is necessary when devel-

oping a new model. Furthermore, implementing a new model without knowing the approximate behaviour of it can cause ICES to crash.

There are differences between the development of the model in MATLAB and the ICES implementation in Fortran, which are discussed and handled in various ways in the upcoming chapter.

3 Methodology

3.1 Combustion model

In this project, a zero-dimensional three-zone model has been developed. As described in sub-section 2.2.3, in this model the combustion chamber is divided into three zones as soon as the combustion process starts. The unburned and burned zones are separated from each other by the flame front zone, and the combustion continues until all the unburned species in the unburned zone are completely burned.

Real gas data is not available in Matlab, and therefore the development of the model in MATLAB is based on approximate values of several parameters such as e.g. individual gas constants or specific heat capacities of the unburned and burned zone. On the other hand, real gas data can be obtained at any time in ICES and the implementation of the model in ICES uses actual gas data.

The engine specifications used for implementation of this combustion model are listed in table 3.

Parameter	Value
Bore [m]	0.131
Stroke [m]	0.158
Connection rod length [m]	0.259
Compression ratio	13

Table 3: Engine specifications

The movement of the flame front depends on the flame speed, which in turn is determined by the laminar and turbulent flame speeds, i.e. S_L and S_T . This means that the flame front propagates a distance dr within each time step dt . The flame radius at any crank angle can be written according to

$$\begin{aligned} dr &= \text{flame speed} \cdot dt \\ r_{flame}(t) &= r_{flame}(t-1) + dr \end{aligned} \quad (31)$$

where dt depend on the engine speed in RPS, revolutions per second, and crank angle sampling frequency and is given by

$$dt = \frac{\text{sampling frequency (CAD)}}{RPS \cdot 360^\circ} \quad (32)$$

The flame speed in equation 31 depends on both the laminar and the turbulent flame speeds. The turbulent flame speed can be calculated in two ways, either according to equation 21 or with help of expression 21, both presented in section 2.3.5. In both equations TI is used, which can be derived from TKE according to equation 20 in section 2.3.4. There is an existing model in ICES for TKE that can be used by the combustion model to include turbulence. With help of this TKE model, TI can be obtained at any time in ICES.

To calculate the laminar flame speed according to the equation 8 in section 2.3.3, the temperature of the unburned zone, T_{un} , and the in-cylinder pressure need to be known.

There are several parameters available in ICES such as BR , burnt ratio, and $BR_{unburned}$, which is the equivalence of FBR that has been mentioned earlier throughout the project. The values of these parameters can be retrieved and used at any time and are updated after each time step in ICES. With help of BR and FBR the mass fractions of the unburned and the burned zone can be calculated according to

$$\begin{aligned}\frac{m_b}{M_{total}} &= \frac{BR - FBR}{1 - FBR} \\ \frac{m_{un}}{M_{total}} &= 1 - \frac{m_b}{M_{total}}\end{aligned}\quad (33)$$

The difference between T_{un} and T_b , ΔT , is then given by

$$\Delta T = \frac{Q_{LHV} \cdot (1 - FBR) \cdot \frac{1}{AFS \cdot \lambda}}{c_{p, avg}} \quad (34)$$

where $c_{p, avg}$ is calculated according to

$$c_{p, avg} = c_{p, un} \cdot \left(1 - \frac{m_b}{M_{total}}\right) + c_{p, b} \cdot \frac{m_b}{M_{total}} \quad (35)$$

Parameters $c_{p, un}$, $c_{p, b}$, and T_{avg} can be retrieved at any time from ICES. These parameters are utilized in equation 36, where replacing T_{un} with $T_b - \Delta T$ leads to equation 37.

$$T_{avg} \cdot M_{total} \cdot c_{p, avg} = T_{un} \cdot m_{un} \cdot c_{p, un} + T_b \cdot m_b \cdot c_{p, b} \quad (36)$$

$$T_b = \frac{\left(\frac{T_{avg} \cdot M_{total} \cdot c_{p, avg}}{m_{un} \cdot c_{p, un}}\right) + \Delta T}{1 + \left(\frac{m_b \cdot c_{p, b}}{m_{un} \cdot c_{p, un}}\right)} \quad (37)$$

It is assumed that the flame has a spherical shape. This means that the geometry of the flame is known and that the volume of the flame can be calculated at any time step. The flame volume calculations have been provided in the next section, section 3.2.

Being able to calculate the volume of the flame gives the possibility to determine how much the flame volume is growing in each time step. This calculation is done according to

$$\Delta V = V_{flame}(t) - V_{flame}(t - dt) \quad (38)$$

ΔV in each time step together with equation 23 gives an approximation of the entrained mass.

The volumes of the unburned zone and the burned zone can be calculated at any time with help of R_b and R_{un} according to equation 39. The values of R_b and R_{un} can be retrieved from ICES for the unburned and the burned zones.

$$\begin{cases} V_b = \frac{m_b \cdot T_b \cdot R_b}{P_{incyl}} \\ V_{un} = \frac{m_{un} \cdot T_{un} \cdot R_{un}}{P_{incyl}} \end{cases} \quad (39)$$

3.2 Flame geometry

Assuming that the flame in the combustion chamber has a spherical shape restricted by interaction with the combustion chamber walls, the volume and area of the flame can be calculated. Flame volume and area depends on the position of the piston, which determines the squish height in the cylinder.

As long as the radius of the flame, r_{flame} , is smaller than half of the cylinder diameter, $\frac{bore}{2}$, the volume and area of the flame can be calculated according to equations 40 and 41. In equation 40, which refers to the geometry shown in figure 2 (a), the volume and area of the flame is estimated as half of the volume and area of a sphere.

$$\begin{cases} V_{flame} = \frac{V_{sphere}}{2} = \frac{2}{3} \cdot \pi \cdot (r_{flame})^3 \\ A_{flame} = \frac{A_{sphere}}{2} = 2 \cdot \pi \cdot (r_{flame})^2 \end{cases} \quad (40)$$

Considering the flame geometry in figure 2 (b), the volume and area of the cap, the portion of the flame that ends up under the piston, need to be subtracted from the volume and area of the sphere. The volume and area of the cap is calculated according to [25].

$$\begin{cases} V_{flame} = \frac{V_{sphere}}{2} - V_{cap} \\ \quad = \frac{2}{3} \cdot \pi \cdot (r_{flame})^3 - \frac{\pi \cdot (h_{cap})^2}{3} \cdot (3 \cdot r_{flame} - h_{cap}) \\ A_{flame} = \frac{A_{sphere}}{2} - A_{cap} = 2 \cdot \pi \cdot (r_{flame})^2 - 2 \cdot \pi \cdot r_{flame} \cdot h_{cap} \end{cases} \quad (41)$$

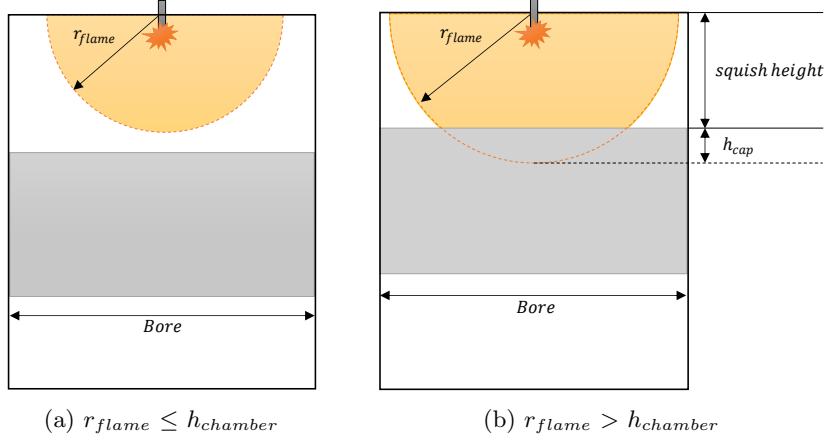


Figure 2: Flame geometry when $r_{flame} \leq \frac{bore}{2}$

As soon as r_{flame} becomes larger than $\frac{bore}{2}$, equations 42 and 43 are used for flame volume and area calculation. Two cases may occur depending on the position of the piston and r_{flame} , which are both shown in figure 3.

In case of the flame geometry in figure 3 (a), the volume and area of the flame is calculated according to equation 42 with help of θ and r_{flame} [25]. For flame geometry in figure 3 (b), the calculation is simpler and is done according to equation 43. The volume of the flame in this case, is simply equal to the volume of the cylinder.

$$\left\{ \begin{array}{l} V_{flame} = \frac{\pi}{3} \cdot (r_{flame})^3 \cdot (2 + \cos \theta) \cdot (1 - \cos \theta)^2 \\ \quad - \frac{\pi \cdot (h_{cap})^2}{3} \cdot (3 \cdot r_{flame} - h_{cap}) + h_{cylindrical} \cdot \pi \cdot \left(\frac{bore}{2}\right)^2 \\ A_{flame} = 2 \cdot \pi \cdot (r_{flame})^2 \cdot (1 - \cos \theta) - 2 \cdot \pi \cdot r_{flame} \cdot h_{cap} \end{array} \right. \quad (42)$$

$$\left\{ \begin{array}{l} V_{flame} = squish\ height \cdot \pi \cdot \left(\frac{bore}{2}\right)^2 \\ A_{flame} = 0 \end{array} \right. \quad (43)$$

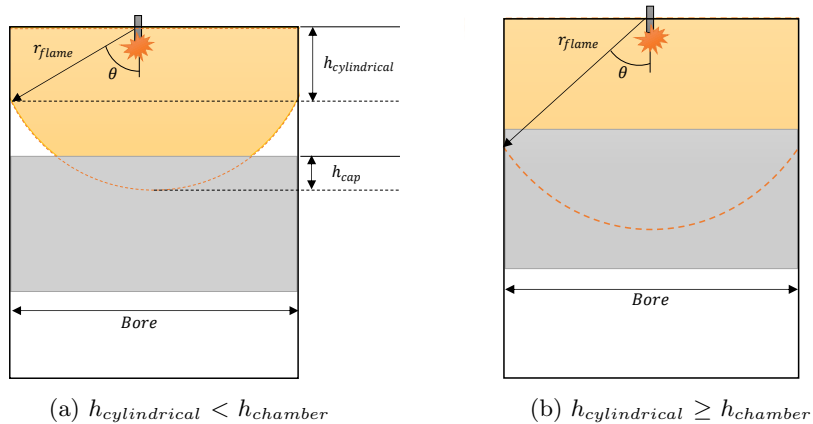


Figure 3: Flame geometry when $r_{flame} > \frac{bore}{2}$

The placement of the spark plug does not necessarily need to be in the middle of the combustion chamber as shown in flame geometry figures of this section. If the spark plug is placed freely e.g. in the right or left corner of the combustion chamber, a certain part of the flame will hit the chamber wall earlier. The flame volume and area are calculated with help of circle-circle intersection in [26], for a freely placed spark plug.

3.3 Laminar flame speed

A model for laminar flame speed has been developed using Cantera with its Python interface. In this model a freely propagating flame of a hydrogen-air mixture has been simulated to evaluate the laminar flame speed for a given ϕ , temperature, pressure, and FBR . This model uses a hydrogen-air detailed chemical reaction model from *UC San Diego University*.

Relevant intervals are chosen for ϕ , temperature, pressure, and FBR . These intervals are 0.2-1 for ϕ , 500-1000 K for temperature, 10-250 bar for pressure, and 0-0.2 for FBR . The Cantera model showed inconsistencies and extremely high laminar flame speeds for temperatures between 900-1000 K . This is probably because of the fact that the autoignition temperature of hydrogen is at 853 K , which is discussed in chapter 5. To avoid this issue in Cantera, the initially chosen interval limits for temperature have been changed to 500-900 K .

The Cantera model for laminar flame speed can be used with its Python interface at any time. However, implementing this model in ICES as a part of the combustion model involves implementation of the entire Cantera toolbox in ICES. This task is tedious and therefore it is important to find a way to calculate the laminar flame speed in ICES without any Cantera implementation.

To calculate the laminar flame speed for any given ϕ , temperature, pressure, and FBR , it is desirable to be able to express the laminar speed in form of equation 8. As mentioned in sub-section 2.3.3, $S_{L,ref}$, α , and β in equation 8 are unknown constants dependent on ϕ . Therefore, it is important to find these constants as they are expressed in equations 9-13.

Using the Cantera model for laminar flame speed and trying out different fitting and optimization tools, give the values of $S_{L,ref}$, α , and β . In this way, it is possible to calculate the laminar flame speed with help of equation 8 and independent of the Cantera model. In this project, two methods have been used which are presented in the following two sub-sections.

Since the model is built on a temperature interval of 500-900 K, the remaining problem is how to deal with temperatures higher than 900 K. The idea here was to develop the laminar flame speed model for the given temperature interval and afterwards evaluate how the model reacts within higher temperature ranges. If the evaluation results do not show the same kind of inconsistency seen in Cantera, the model can be used even for higher temperatures.

3.3.1 Method 1 - Fitting separately

According to [17], the influence of each term in equation 8 on laminar flame speed can be kept and studied separately. This means that if dilution is assumed to be negligible, and T_{un} and P_{incyl} are equal to T_{ref} and P_{ref} , the influence of the $S_{L,ref}$ term can be expressed as in equation 44. Knowing S_L from Cantera for various ϕ values and using equation 44, makes it possible to calculate C_1 , C_2 , and C_3 . This is done in the curve fitting tool in MATLAB, where S_L and ϕ are the input variables. Equation 44 is used as a custom equation to fit the input data to the equation.

$$S_L = S_{L,ref} = C_1 + C_2 \cdot (\phi - C_3)^2 \quad (44)$$

Furthermore, the influence of temperature and pressure on the laminar flame speed can be expressed according to equations 45 and 46. Constants T_1 - T_5 and P_1 - P_5 are found in the same manner as for C_1 - C_3 and by treating each term separately.

$$S_L = \left(\frac{T_{un}}{T_{ref}} \right)^\alpha = \left(\frac{T_{un}}{T_{ref}} \right)^{(T_1 + T_2 \cdot \phi + T_3 \cdot \phi^2 + T_4 \cdot \phi^3 + T_5 \cdot \phi^4)} \quad (45)$$

$$S_L = \left(\frac{P_{incyl}}{P_{ref}} \right)^\beta = \left(\frac{P_{incyl}}{P_{ref}} \right)^{(P_1 + P_2 \cdot \phi + P_3 \cdot \phi^2 + P_4 \cdot \phi^3 + P_5 \cdot \phi^4)} \quad (46)$$

Since this fitting method is done around a reference temperature, T_{ref} , and a reference pressure, P_{ref} , and each term is treated separately, any deviation from these reference values can result in misleading outcomes. This will be addressed and discussed in detail in section 4.1.1.

3.3.2 Method 2 - Fitting simultaneously

As it will be shown in section 4.1.1, method 1 did not give a laminar flame speed model that was sufficiently accurate. For this reason, an alternative method is represented in this section. This method is based on fitting the influencing terms in the laminar flame speed equation simultaneously with help of *fmincon*.

fmincon aims to find a minimum of a nonlinear multivariable function. This is used to minimize the error expressed in equation 47, which is essentially the difference between the S_L values calculated by Cantera and S_L values calculated according to equation 8. N is the number of the input data points and a data point is a set of specific ϕ , T_{un} , P_{incyl} , and FBR .

$$error = \frac{\sqrt{\sum((S_{L,Cantera} - S_L)^2)}}{N} \quad (47)$$

By using this optimization method for laminar flame speed, all four terms of equation 8, namely $S_{L,ref}$, the temperature influence (equation 45), the pressure influence (equation 46) and even $f(dilution)$, can be included in the optimization at the same time. The dilution effect on laminar flame speed, $f(dilution)$, has been expressed before in section 2.3.3 according to equation 10. This equation is in fact a polynomial of degree seven and the constants such as 1 or 0.75 can be replaced with arbitrary constants. $f(dilution)$ is therefore rewritten according to equation 48 with arbitrary constants D_1 - D_8 , and used in this form in the optimization.

$$f(dilution) = D_1 + D_2 \cdot FBR + D_3 \cdot FBR^2 + D_4 \cdot FBR^3 + D_5 \cdot FBR^4 + D_6 \cdot FBR^5 + D_7 \cdot FBR^6 + D_8 \cdot FBR^7 \quad (48)$$

It is preferable for the input data points to be randomly chosen in relevant intervals for ϕ , T_{un} , P_{incyl} , and FBR . Therefore, a four-dimensional matrix with random points has been generated using the Latin Hypercube sample matrix function, *lhsdesign*, in MATLAB. This matrix initially contained 100 data points and was afterwards extended to contain 1000 data points. The intervals used for ϕ , T_{un} , P_{incyl} , and FBR are 0.2-1, 500-900 K, 10-250 bar, and 0-0.2, respectively.

The matrix is fed into the laminar flame speed model in Cantera and the result is used in optimization according to equation 47. *fmincon* then tries to minimize the error and returns the values of constants C_1 - C_3 , T_1 - T_5 , P_1 - P_5 , and D_1 - D_8 after the optimization is completed.

3.4 Implementation and setup in ICES

3.4.1 Implementation in Fortran

When the implementation of the combustion model is completed in MATLAB and the results are satisfactory, this code is translated to Fortran for implementation in ICES. There are several distinctions between the implementation in MATLAB and Fortran. The most important one regarding this project is that matrix operations are complicated in Fortran compared to MATLAB.

The problem that has been encountered during the transition from MATLAB to Fortran was not being able to retrieve the flame radius for the previous time step, which has been done in MATLAB by using matrix operations. The flame volume can be calculated from the unburned zone and the burned zone masses,

which enables the possibility to compute the flame radius from the flame volume at the previous time step. Yet, it is not a straightforward task to calculate flame radius from flame volume.

A two-dimensional matrix with randomly chosen points has been generated using *lhsdesign* in MATLAB. The two dimensions are the radius and the squish height since the value of cylinder bore is always the same considering a specific cylinder geometry. This matrix is fed into the volume routine to calculate the flame volume. This flame volume has afterwards been used to calculate the flame radius with help of various methods. Three different methods has been tested for this purpose, which are based on a regression model, radial basis and an iterative solution.

The first method uses a cubic regression model which depends on two input parameters, the radius and the squish height. Radial basis has been used as a second alternative method to calculate flame radius [27].

The iterative solution uses Secant method to find the flame radius that gives a certain volume. Secant method is a recursive method to find a root of a function by successive approximation [28].

3.4.2 ICES setup in GUI

In ICES, the implementation of a single cylinder spark-ignition combustion engine looks as shown in figure 4. The inlet and exhaust valve lifts are shown in figure 5.

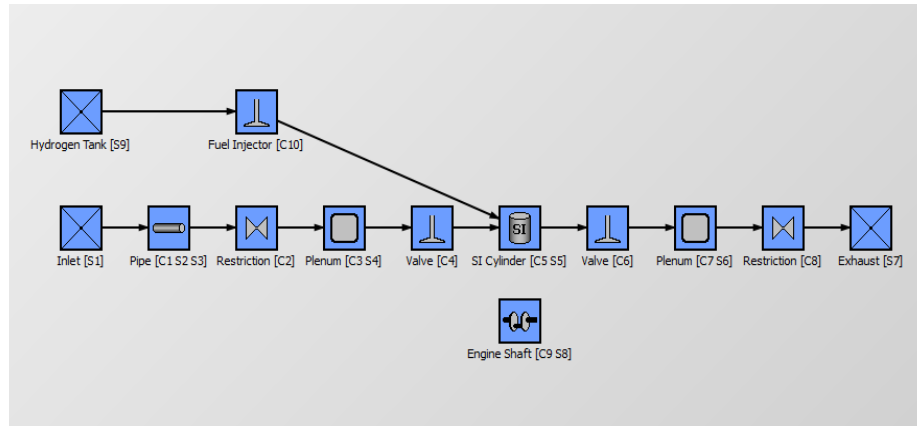


Figure 4: ICES GUI

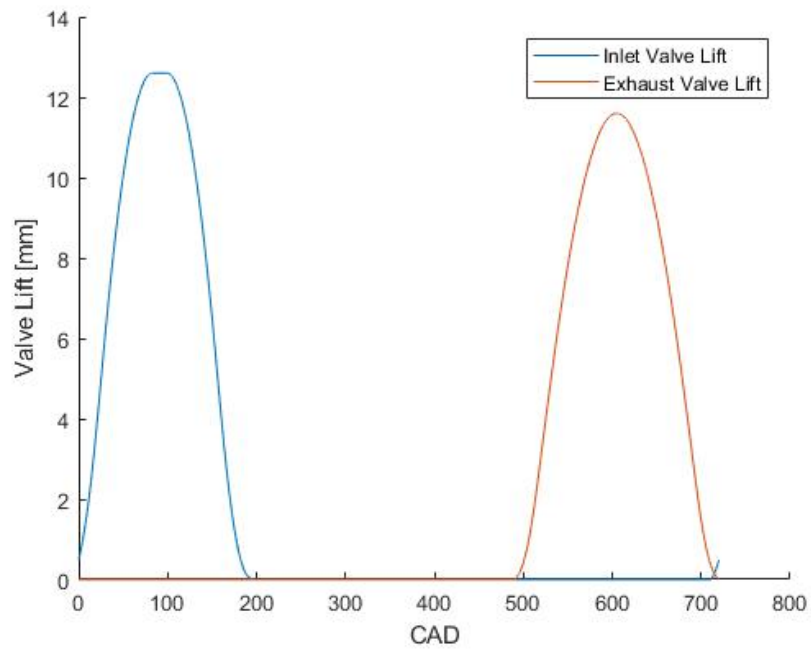


Figure 5: ICES inlet and exhaust valve lifts

4 Results

4.1 Laminar flame speed

The Cantera model for laminar flame speed has been simulated initially for ϕ values between 0.25-1.8, and the result is shown in figure 6. In this simulation, the initial temperature and pressure are set to 298 K and 1 bar at the same time as FBR is zero.

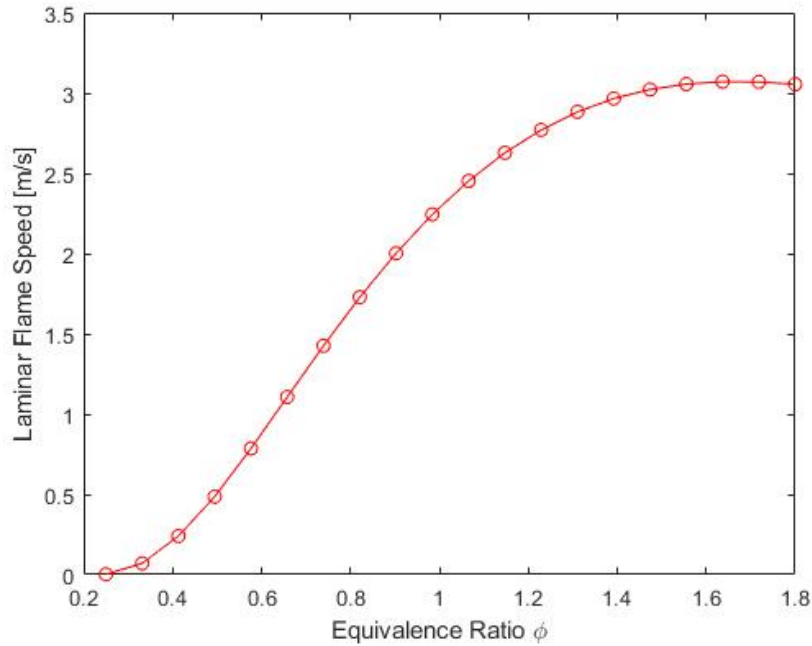


Figure 6: Laminar flame speed as a function of equivalence ratio, ϕ

The results of the laminar flame speed model in Cantera have been compared to the experimental data found in [29]. This is shown in table 4 for equivalence ratios equal to 0.5, 1, and 1.5.

ϕ	Cantera model	Verhelst 2005 [29]	Bradley 2007 [29]	Pareja 2010 [29]
0.5	0.52	0.64	0.66	–
0.8	1.66	1.60	1.70	1.70
1	2.33	2.30	–	2.38
1.5	2.89	–	–	3.10

Table 4: Comparison between the laminar flame speed in Cantera and experimental data found in literature

To be able to see the temperature influence on laminar flame speed, the pressure is kept with its initial value of 1 bar simultaneously as the temperature and ϕ values vary. The same has been done to see the pressure influence on the laminar flame speed. The results are presented in figures 7 and 8.

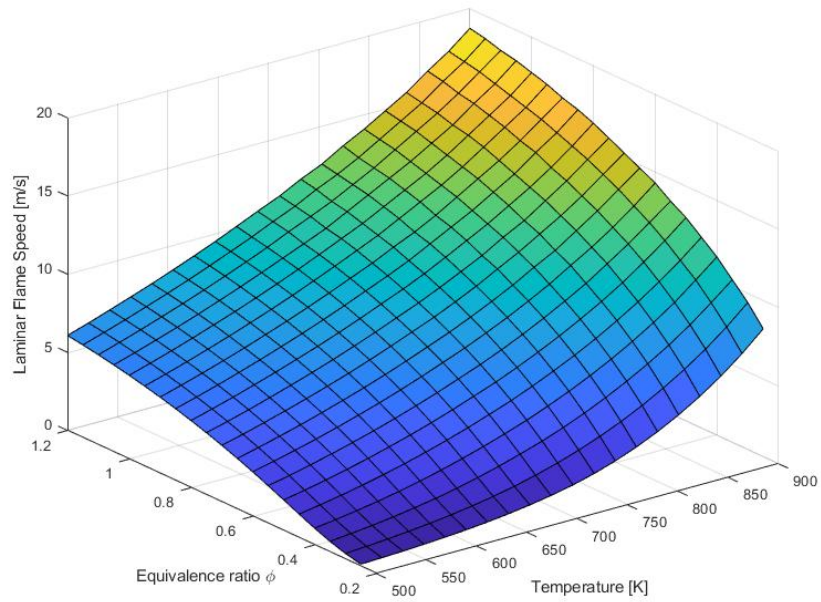


Figure 7: Laminar flame speed dependency on temperature and ϕ at 1 bar

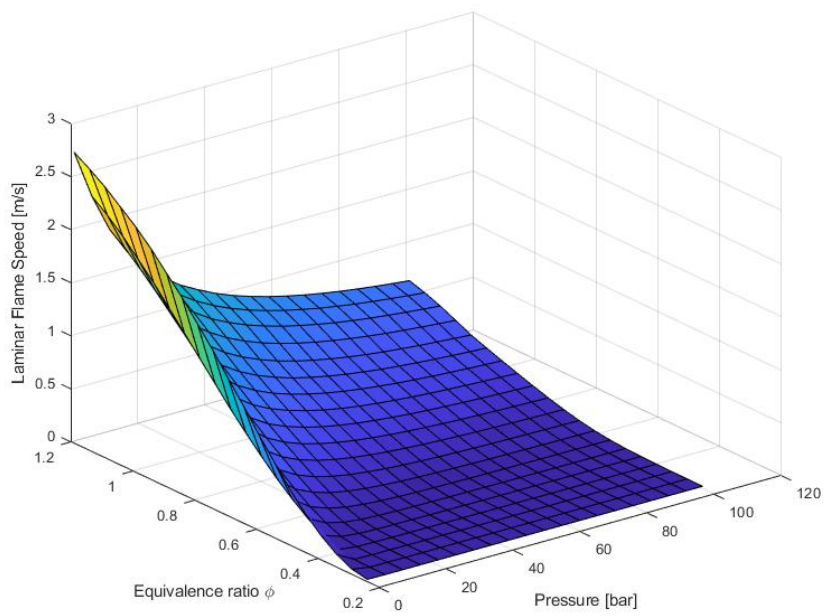


Figure 8: Laminar flame speed dependency on pressure and ϕ at 298 K

4.1.1 Results of method 1 - Fitting separately

The first attempt to fit equation 44 to the input data is shown in figure 9. The blue line shows the input data, which is the laminar flame speed values calculated by Cantera. The red dashed line is the result of the curve fitting, which shows the predicted laminar flame speed values calculated using equation 44 and replacing $C1-C3$ with the values retrieved from curve fitting. As seen in this figure, a polynomial of degree two is not the most suitable option for fitting in this case.

Therefore, equation 44 is replaced with a polynomial of degree four for a better match. The new equation, equation 49 with constants $C1-C5$, is then used as the custom equation to try to fit to the input data. The result, shown in figure 10, shows a very accurate match.

$$S_L = S_{L,ref} = C_1 + C_2 \cdot \phi + C_3 \cdot \phi^2 + C_4 \cdot \phi^3 + C_5 \cdot \phi^4 \quad (49)$$

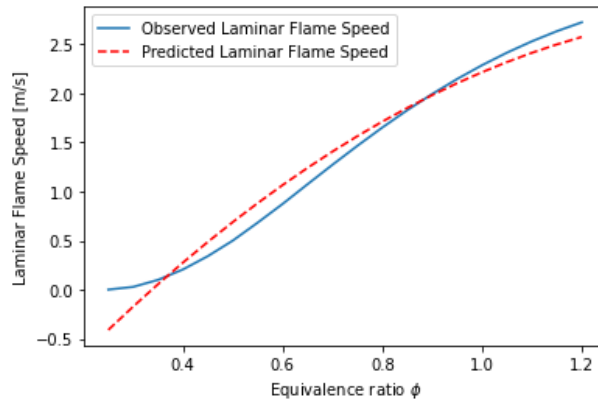


Figure 9: Method 1: Result for fitting $S_{L,ref}$ using equation 44

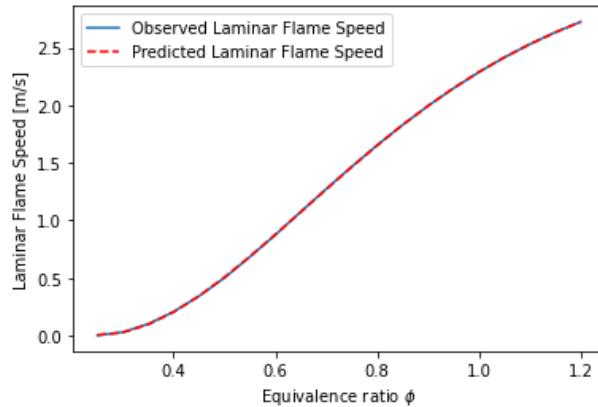


Figure 10: Method 1: Result for fitting $S_{L,ref}$ using equation 49

Using the temperature influence on laminar flame speed from Cantera, MATLAB's curve fitting tool is then used to fit a curve to this data using equation 45. The result is shown in figure 11 and a R-square value equal to 0.9613 is achieved.

R-square, R^2 , is known as the coefficient of determination, which is basically a measure for indicating the goodness of the fit of the model. A R-square value of 0.9613 means that 96 % of the variation in the output is explained by the input variable.

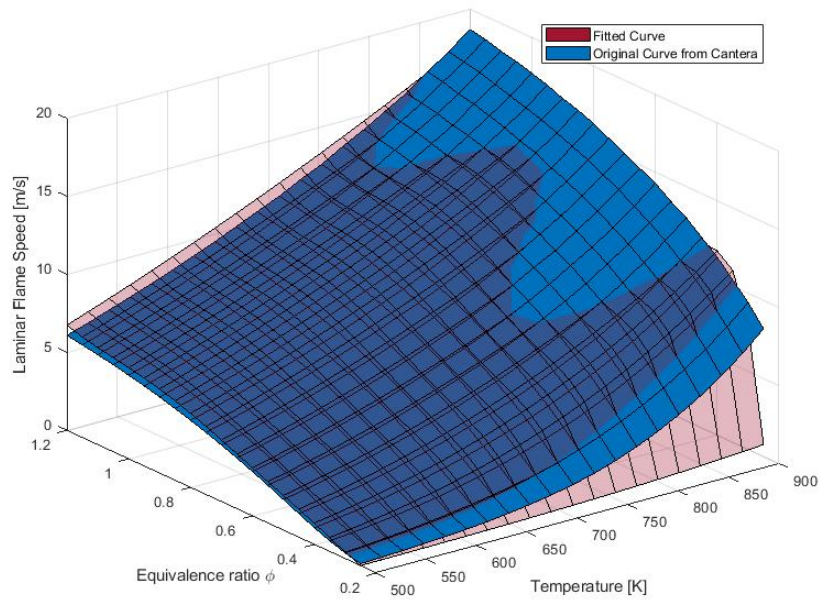


Figure 11: Method 1: The temperature fit

In the same way, the pressure influence on laminar flame speed has been used for curve fitting according to equation 46. The result is shown in figure 12 and a R-square value equal to 0.9573 is achieved.

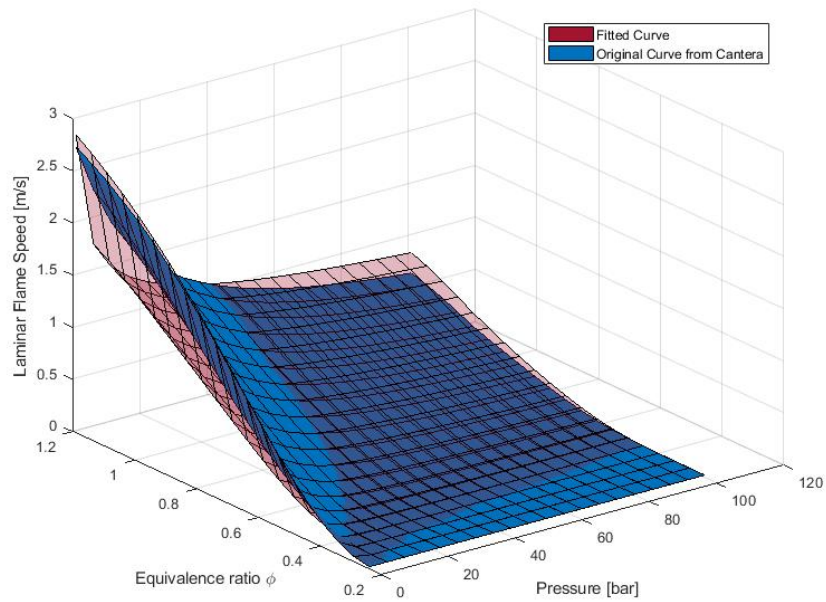
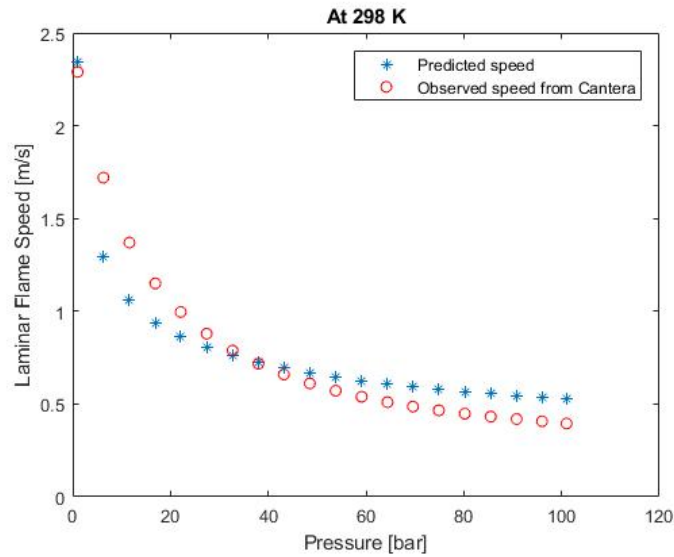
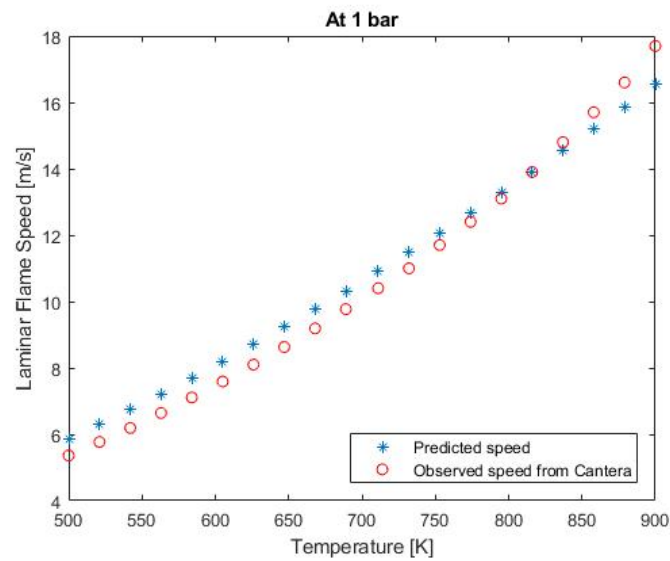


Figure 12: Method 1: The pressure fit

To be able to evaluate the results of curve fitting attempt, the observed laminar flame speed is plotted together with the predicted flame speed values by either keeping temperature constant and varying pressure or vice versa. As long as the temperature and pressure are kept near to the reference values of 298 K and 1 bar , the difference between the observed and predicted laminar flame speed values is not extreme. This is shown in figure 13.



(a) Evaluation of pressure dependency of laminar flame speed at reference temperature

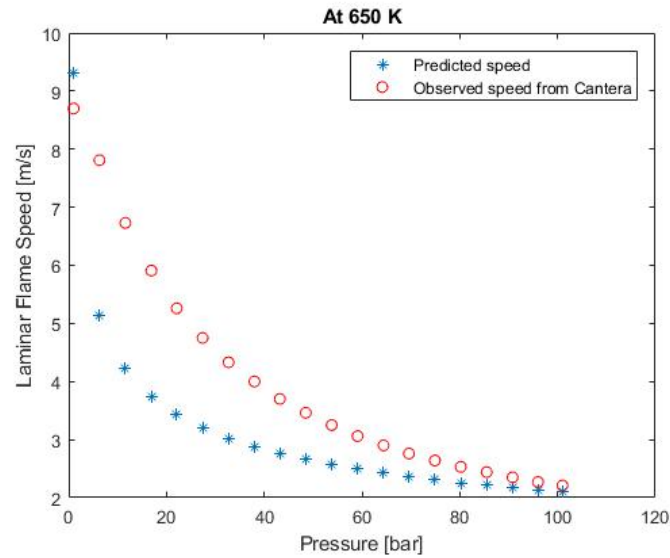


(b) Evaluation of temperature dependency of laminar flame speed at reference pressure

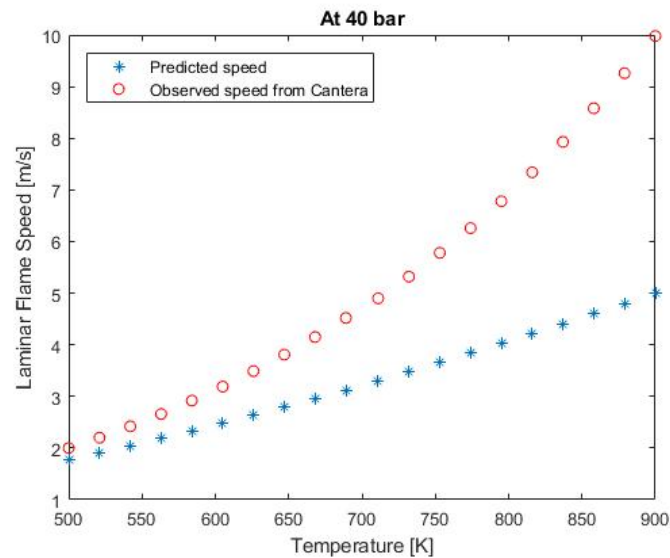
Figure 13: Method 1: Laminar flame speed evaluation at the reference conditions

On the other hand, figure 14 (a) shows the observed and predicted laminar flame speed values at 650 K, approximately 350 degrees from the reference temperature. Now, there are extremely large difference between the observed and predicted values, which indicates that the model is not functioning well when the temperature and pressure vary from the reference values. The same

kind of result can be seen in figure 14 at 40 *bar*.



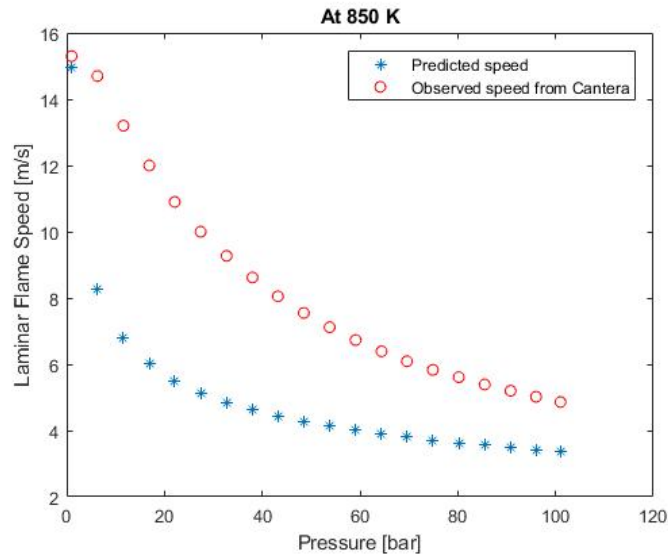
(a) Evaluation of pressure dependency of laminar flame speed at 650 *K*



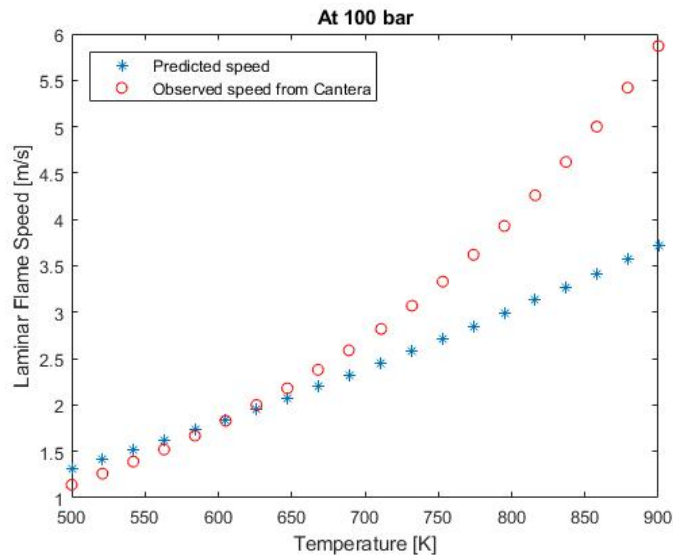
(b) Evaluation of temperature dependency of laminar flame speed at 40 *bar*

Figure 14: Method 1: Laminar flame speed evaluation at conditions differing from the initial conditions

Figure 15 (a) shows the observed and predicted laminar flame speed values this time at 850 *K*, 550 degrees from the reference temperature. At 100 *bar* and varying temperatures, the result can be seen in figure 15 (b).



(a) Evaluation of pressure dependency of laminar flame speed at 850 K



(b) Evaluation of temperature dependency of laminar flame speed at 100 bar

Figure 15: Method 1: Laminar flame speed evaluation at conditions differing from the initial conditions

In the final evaluation, a set of points with randomly chosen equivalence ratio, temperature and pressure is used to calculate the laminar flame speed according to the results of fitting separately. The evaluation result is plotted in figure 16, in which the predicted laminar flame speed is the calculated speed and the observed laminar flame speed is the speed evaluated in Cantera. The deviations are not acceptable specifically since they occur at pressures and temperatures

within the area that is interesting in this project. This method is therefore not used further in this project.

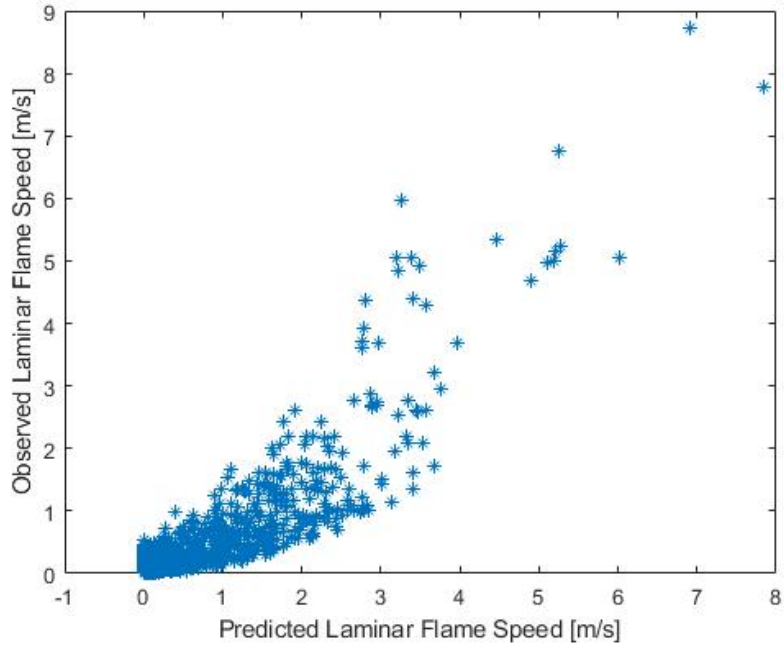


Figure 16: Method 1: Observed vs predicted laminar flame speed

4.1.2 Results of method 2 - Fitting simultaneously

Figure 17 shows the observed and predicted laminar flame speeds against each other after the optimization has succeeded. In this optimization, 100 random data points have been used as the training data. As the figure demonstrates, the predicted values for laminar flame speed are almost the same as the observed values. This indicates that this method gives more accurate results in comparison to the method used in the previous section, section 4.1.1.

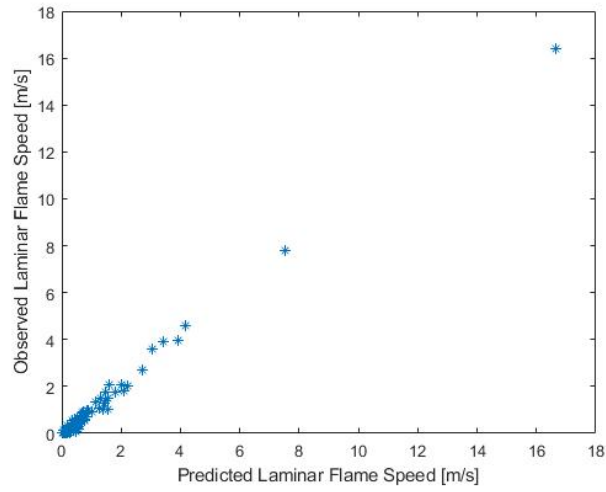


Figure 17: Method 2: Observed vs predicted laminar flame speed (training data contain 100 data points)

Because this method proved to give accurate results, the optimization was done once more with a training data containing 900 data points instead of just 100 points. The result is shown in figure 18 and is satisfactory.

The values of coefficients C_1-C_3 , T_1-T_5 , P_1-P_5 , and D_1-D_8 are returned as the result of optimization and can be used to calculate laminar flame speed for any arbitrary data point. These values are specified in table 5. To evaluate the model, 110 random data points have been used as the validation data, which are separate from the training data. For the validation data the laminar flame speed has been calculated and plotted against the the laminar flame speed values from Cantera. This can be seen in figure 19.

Coefficient	Value
$C1$	-23.3476
$C2$	3.4653
$C3$	-2.4232
$T1$	1.9334
$T2$	0.2441
$T3$	-0.5478
$T4$	-0.4605
$T5$	2.3039
$P1$	1.7016
$P2$	-0.7136
$P3$	-1.0377
$P4$	0.8570
$P5$	-1.4239
$D1$	1.0144
$D2$	1.0102
$D3$	0.9958
$D4$	0.9665
$D5$	1.0559
$D6$	2.1421
$D7$	-0.9833
$D8$	0.1399

Table 5: Values of the coefficients C_1 - C_3 , T_1 - T_5 , P_1 - P_5 , and D_1 - D_8

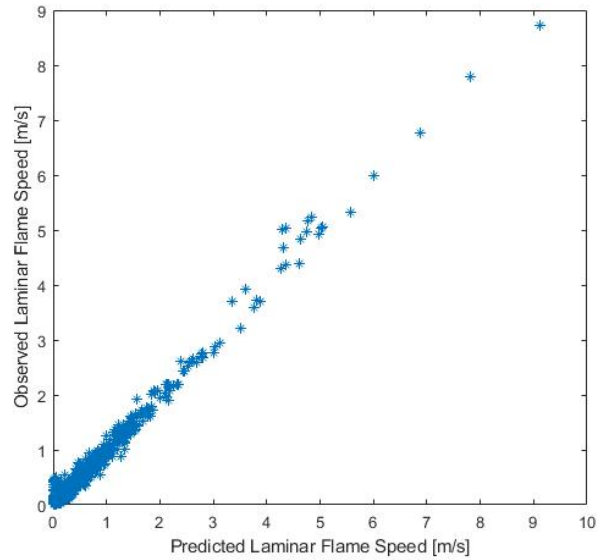


Figure 18: Method 2: Observed vs predicted laminar flame speed (training data contain 900 data points)

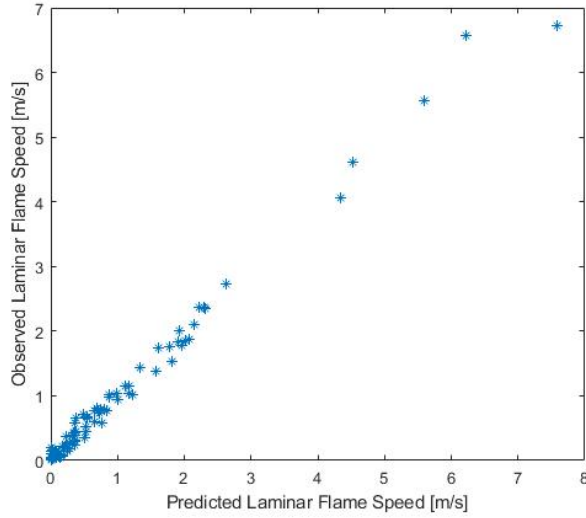
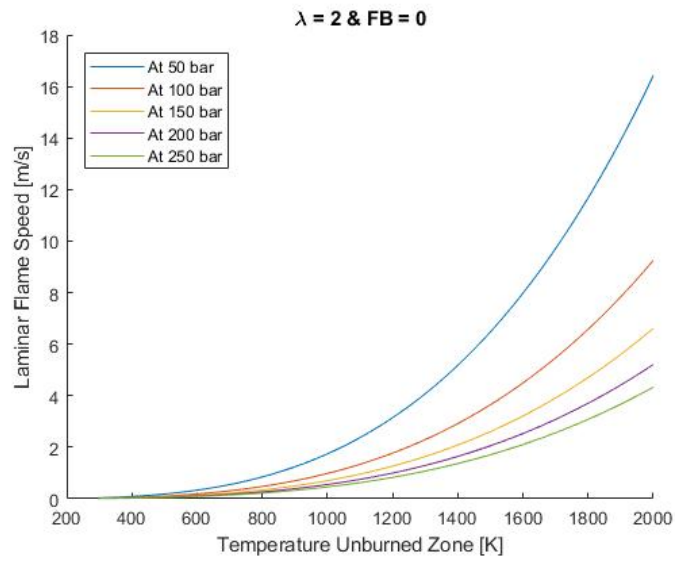


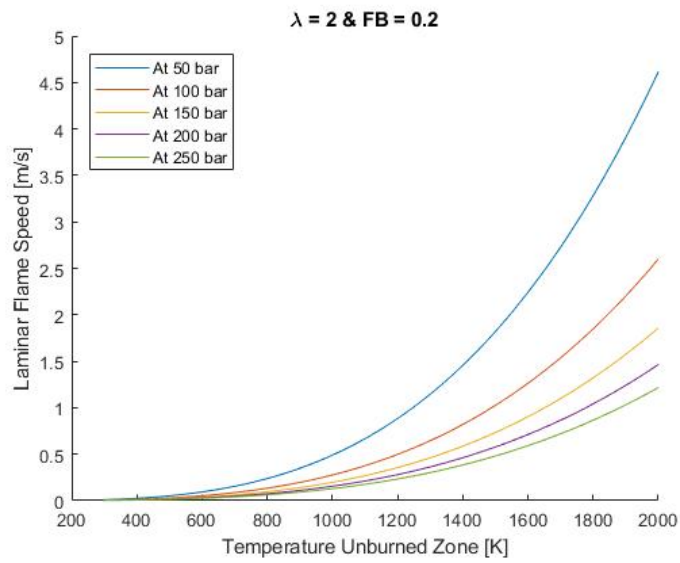
Figure 19: Method 2: Observed vs predicted laminar flame speed (evaluation of validation data)

To further improve the results of the optimization, 500 random data points have been added to the previous 900 data points used in the optimization. This time, these new 500 points represent a focus area where the intervals chosen for ϕ , T_{un} , P_{incyl} , and FBR are much smaller. ϕ , T_{un} , P_{incyl} , and FBR vary between 0.25-0.5, 700-900 K, 90-150 bar, and 0-0.1 respectively in this focus area. The chosen limits for these intervals depend on the values of ϕ , T_{un} , P_{incyl} , and FBR that are most interesting for the final simulation.

The temperature interval used to model laminar flame speed was 500-900 K due to the limitations based on the Cantera model. However, the unburned zone temperature can reach higher temperatures than 900 K. Therefore, the laminar flame speed model has been simulated when the unburned zone temperature exceeds the temperature limits of the model. If the model keeps the same tendency after 900 K and does not show any strange behaviour, it is deemed to be good enough to be used even when the unburned zone temperature is higher than 900 K. This evaluation has been done for two different values of equivalence ratio, $\phi = 0.5$ and $\phi = 0.25$, and for each ratio with and without presence of FBR . The results are presented in figures 20 and 21, and show no strange tendencies in the laminar flame speed model.

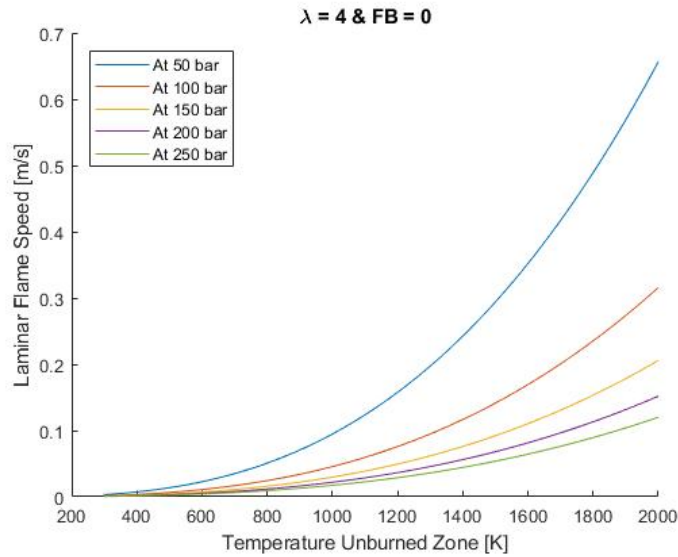


(a) Evaluation of laminar flame speed at higher temperatures without FBR

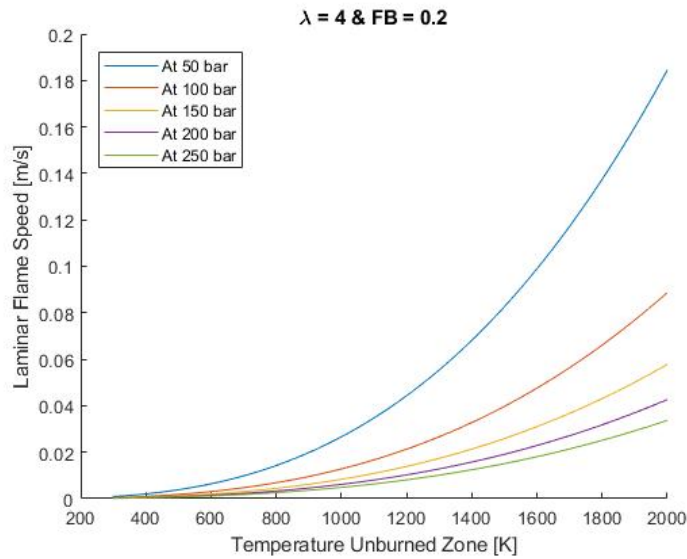


(b) Evaluation of laminar flame speed at higher temperatures with FBR

Figure 20: Method 2: Laminar flame speed at higher temperatures at $\phi = 0.5$



(a) Evaluation of laminar flame speed at higher temperatures without FBR



(b) Evaluation of laminar flame speed at higher temperatures with FBR

Figure 21: Method 2: Laminar flame speed at higher temperatures at $\phi = 0.25$

4.2 Implementation in ICES

4.2.1 Three methods to calculate flame radius

As described earlier, the flame volume can be calculated with an analytic expression as a function of flame radius, bore, and squish height. However, in ICES it is necessary to calculate the flame radius based on the flame volume,

bore, and squish height. It is complicated to derive an analytical expression for this purpose and for this reason three different methods were tested.

The result of the regression model is presented in figure 22. The volume shown on the y-axis as the observed volume is the reference volume, calculated by the volume routine in MATLAB with a given radius and squish height. The regression model predicts a flame radius that corresponds to the observed volume. This predicted radius is then used to calculate a volume, the predicted volume on the x-axis, to evaluate how close the predicted volume is to the original volume. The regression model is fast and easy to implement in Fortran. However, the result is poor and not satisfactory for this part of the project.

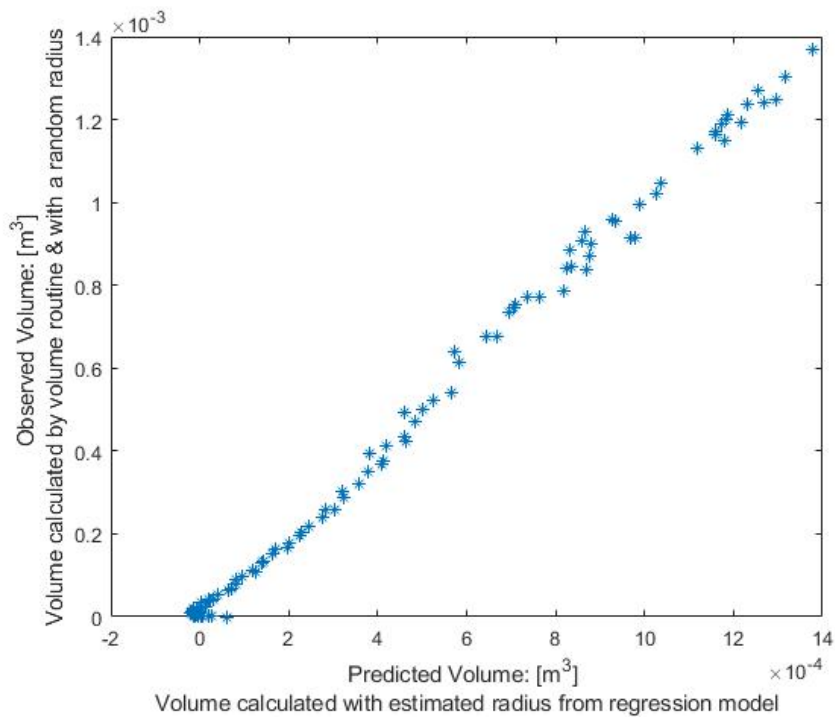


Figure 22: Observed vs predicted volume: Results of regression model

An alternative method has been used based on radial basis, and the results are shown in figures 23 and 24. This method shows perfect result and can be used to calculate the flame radius. However, using this method means dealing with large matrices, which is not quick to do in Fortran.

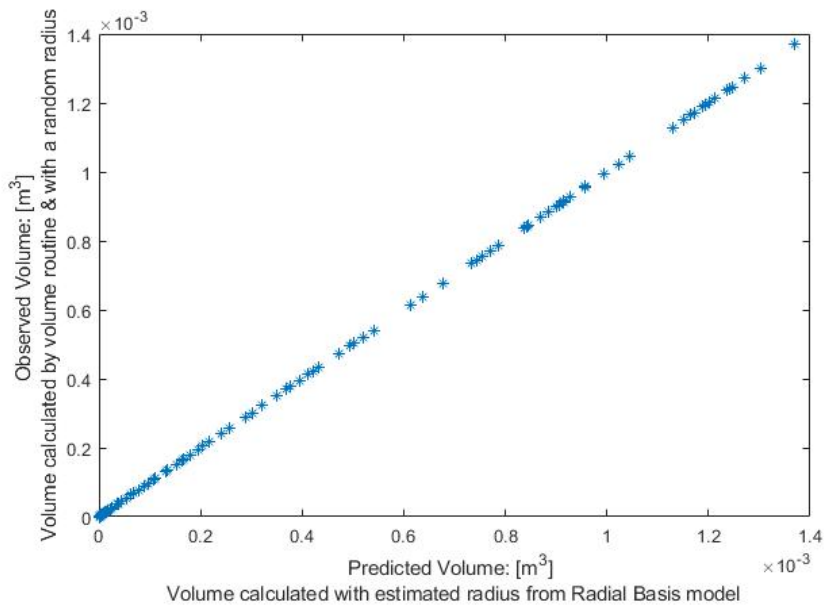


Figure 23: Observed vs predicted volume: Results of radial basis

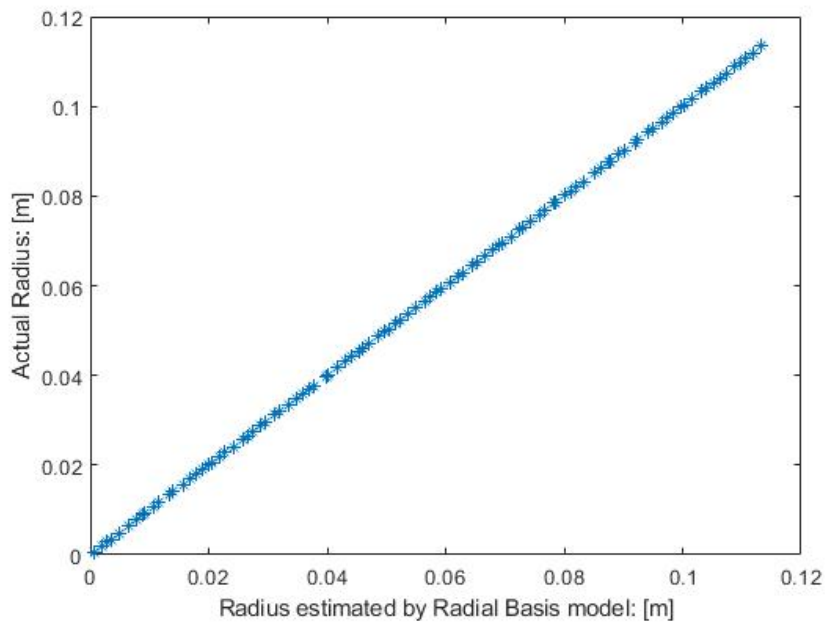


Figure 24: Observed vs predicted radius: Results of radial basis

The third method used to calculate the flame radius is the iterative solution where the radius is calculated by repeatedly trying to minimize the different between the target volume and an approximate guessed volume. The result is

shown in figure 25. This method shows as perfect result as when radial basis was used. In addition, this method is easier to implement in Fortran since it does not deal with large matrices and contain less code.

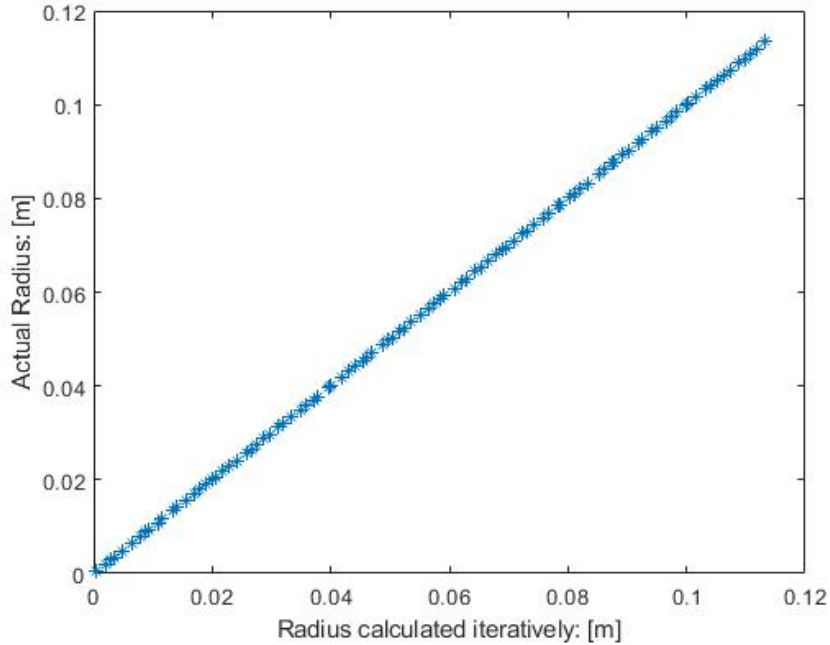


Figure 25: Observed vs predicted radius: Results of the iterative solution

Both iterative solution and radial basis method showed desired outcome. A comparison has been done between these two methods to evaluate how quick each method is. Both methods have been used to evaluate 1000 samples in MATLAB and the elapsed time has been documented. It took 0.083135 seconds for radial basis model and 0.003197 seconds for the iterative solution. The comparison shows that the iterative solution is faster, and this together with the fact that it is simpler to implement in Fortran, makes the iterative solution the winning method.

To make sure that the volume and radius calculation in Fortran works as desired, an evaluation has been done. The flame volume and the calculated radius with the iterative solution from Fortran are restored and the radius is fed into the volume routine in MATLAB. The volume from Fortran is then plotted together with the volume calculated in MATLAB as a function of flame radius, which is shown in figure 26. Both volumes are the same, which indicates that the iterative solution for computing flame radius gives satisfactory result.

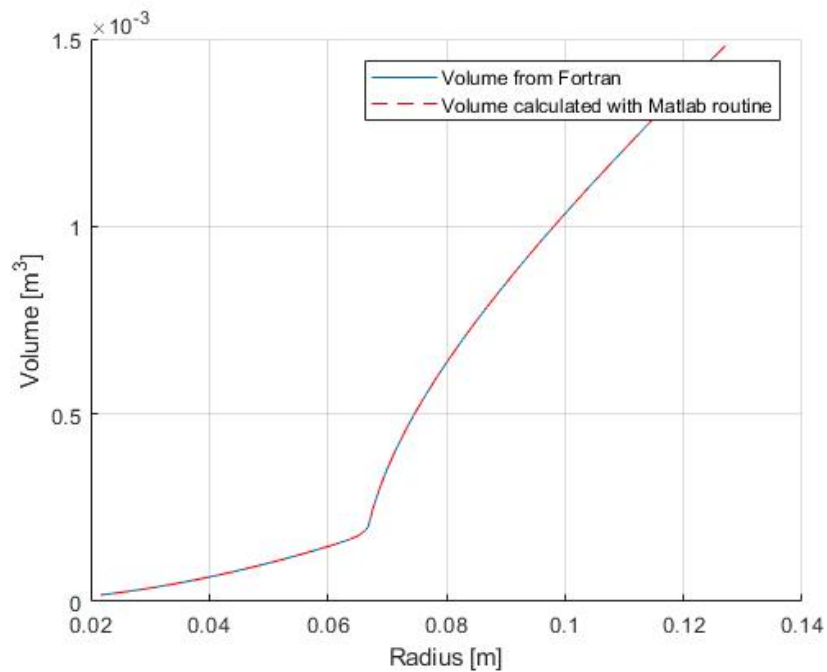
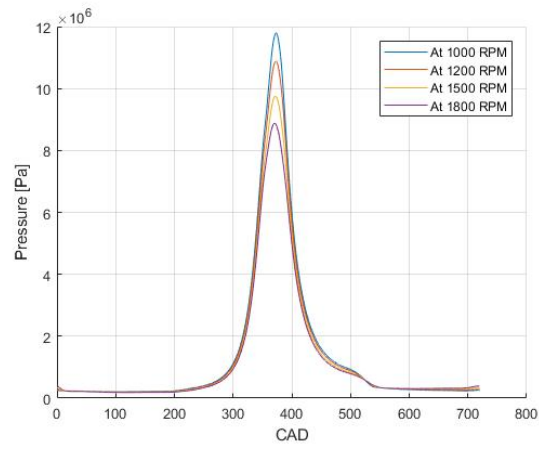


Figure 26: Comparison between flame volume from Fortran vs MATLAB

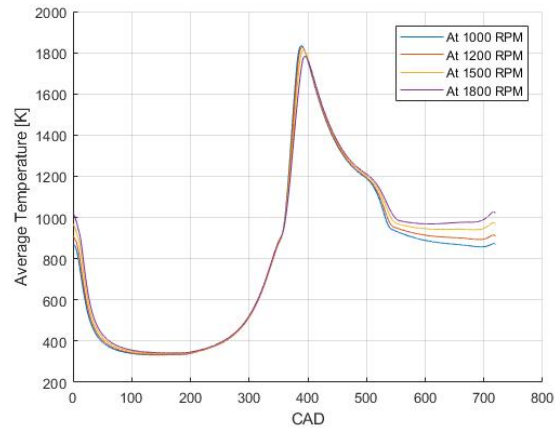
4.2.2 Simulation results in ICES

The results of the model simulation are represented in form of parameter sweep. The parameter sweep has been done by changing only one parameter during several simulations while keeping all the other parameters constant. The model is not calibrated and the purpose of these parameter sweeps is to ensure that the model reacts in a reasonable way to the change of different parameters.

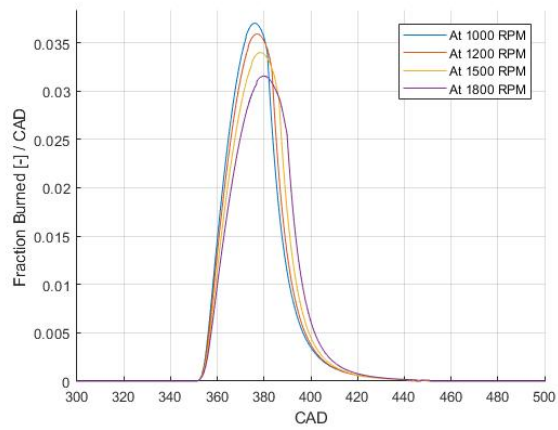
Figure 27 show the in-cylinder pressure, average in-cylinder temperature, and heat release rate as fraction burned per *CAD* for engine speed sweep. In this simulation λ is equal to 2.22 and ignition angle is 350 *CAD* with an ignition delay of 1 *CAD*.



(a) Pressure



(b) Average in-cylinder temperature

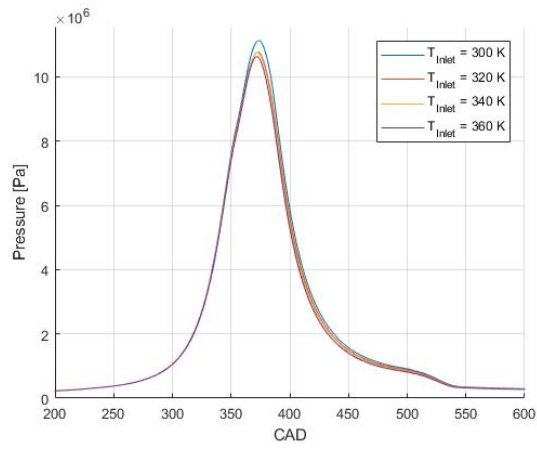


(c) Fraction Burned per CAD, $\frac{FB}{CAD}$

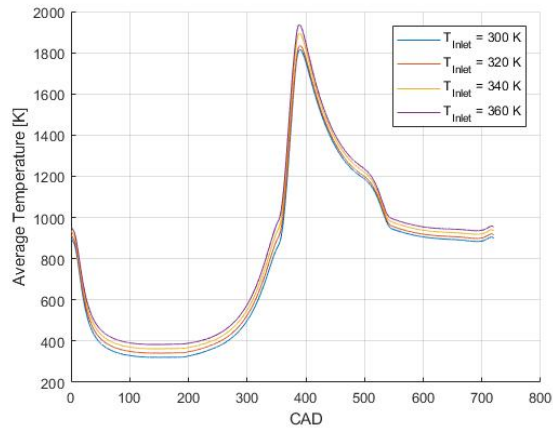
Figure 27: Engine Speed Sweep

Figure 28 show the in-cylinder pressure, average in-cylinder temperature, and heat release rate as fraction burned per *CAD* for temperature sweep, where the inlet temperature vary. In this case the engine speed is held constant at 1200 *RPM* and λ , ignition angle and ignition delay are the same as for the previous simulation.

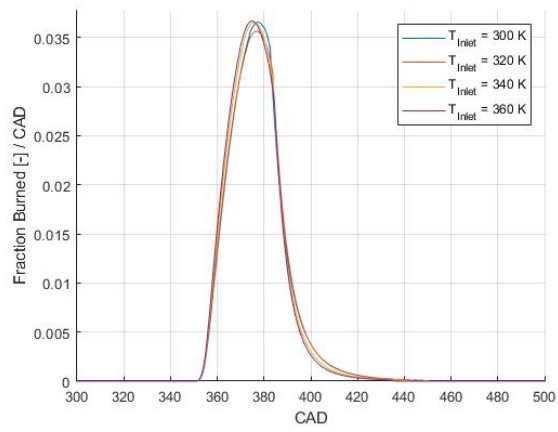
Another parameter sweep has been done, where the inlet and exhaust pressure vary over several simulations while all the other boundary parameters are constant. This is represented in figure 29.



(a) Pressure

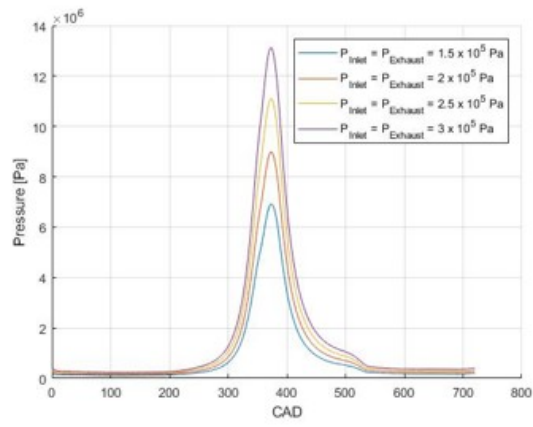


(b) Average in-cylinder temperature

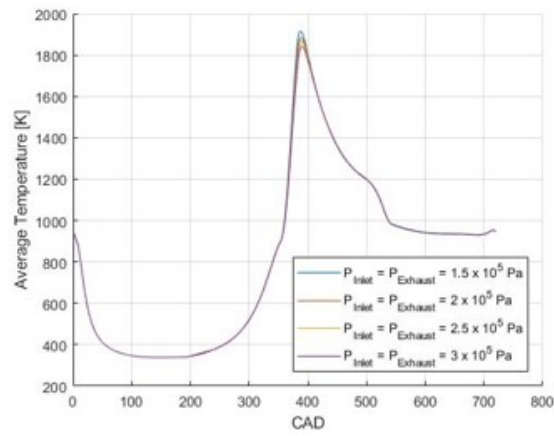


(c) Fraction Burned per CAD, $\frac{FB}{CAD}$

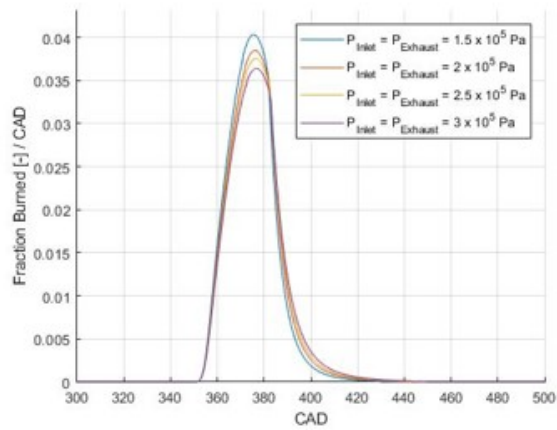
Figure 28: Inlet Temperature Sweep



(a) Pressure



(b) Average in-cylinder temperature



(c) Fraction Burned per CAD, $\frac{FB}{CAD}$

Figure 29: Inlet and Exhaust pressure Sweep

5 Discussion

It has been possible to obtain a great amount of data specifically for laminar flame speed by using Cantera. However, Cantera showed unusually high laminar speeds when the model was used with unburned zone temperatures, T_{un} , higher than 900 K. Not only can the Cantera model itself be the source for this unusual behavior, but the selected chemical-kinetics mechanism for hydrogen-air combustion can have an impact on the results. However, considering the autoignition temperature of hydrogen, which is 853 K, the author believes that the source of the high speeds in Cantera can be due to the fact that the unburned zone temperature reaches and passes 853 K.

What happens when T_{un} starts to approach 853 K and how the combustion process looks like at temperatures higher than the autoignition temperature, are unclear at the moment. It is therefore advisable to take a closer look into this matter in the future.

There are many chemical-kinetics mechanisms available in literature and some have been validated at engine conditions. Trying a previously validated mechanism in Cantera to calculate the laminar flame speed can be done in the future to compare with the existing results. The author recommends doing this as a future work since it can lead to improvements in the laminar flame speed model.

The idea of using the data from Cantera as a reference for the laminar flame speed equation fit proved to be successful. However, treating the influencing variables separately did not give acceptable results. The impact of dilution on laminar flame speed for this method, method 1, was not explored since it would not contribute to any model enhancement. To investigate dilution influence, the model could have been simulated with varying dilution at a reference temperature and pressure. The result would have possibly been acceptable around the reference temperature and pressure similarly to the current results. However, somewhat away from T_{ref} and P_{ref} the results would not be acceptable.

The methodology to model the laminar flame speed when T_{un} , P_{incyl} , and FBR change simultaneously showed a huge improvement compared to when T_{un} and P_{incyl} were treated separately. Both the author and the supervisors found the results of the current model to be satisfactory with minor errors. The fact that turbulent flame speed have a greater impact on flame propagation in comparison to laminar flame speed, makes the effect of these minor errors on the final result to be negligible.

The reference temperature and pressure, T_{ref} and P_{ref} , when calculating the laminar flame speed were set to 298 K and 1 bar, respectively. However, other values could have been chosen that are more relevant at engine conditions. This can additionally be done as future work to investigate whether or not it leads to improvements in the laminar flame speed model.

The flame geometry calculation takes into account the arbitrary position of the spark plug. These calculations have been done assuming spherical flame front and cylindrical piston with a flat head. Other piston geometries e.g. non-cylindrical shapes or recessed piston head, have not been considered. This can be done in the future to improve flame geometry calculations to cover piston bowls, complex piston geometries, etc.

As mentioned before, an existing *TKE* model in ICES has been used to determine the impact of turbulence on the flame speed. However, this model needs to be calibrated with help of data from e.g. CFD simulations.

The author was not able to get hold of reliable test data during the course of this project. Therefore, the main focus has been on developing the model, and calibration and validation will be done in the future work. Sensitivity analysis can additionally be done in the future to study how various sources of uncertainty in the input data contribute to the model's overall behavior.

After the thesis presentation, a couple of articles were suggested to the author where the coefficients in the laminar flame speed correlation were presented for hydrogen. In [30], the authors present a constant value for α , independent of the equivalence ratio, which is valid when T_{ref} is at 298 K. On the other hand, the proposed expressions for $S_{L,ref}$ and β are dependent on ϕ and split in two equivalence ratio domains.

Another set of correlation for laminar flame speed is given in [31]. In this case, T_{ref} is 365 K and P_{ref} is 5 bar, and the coefficients $S_{L,ref}$, α , and β are represented. In [32], an alternative formulation for the laminar flame speed correlation is proposed because the authors believe that the effects of ϕ , P , T , and dilution are not independent and there is a strong interaction between e.g. ϕ and P .

It is strongly recommended to compare the results of the laminar flame speed model in this project with the results presented in [30], [31], and [32] in the future.

6 Conclusion

In this project, a zero-dimensional predictive model for hydrogen combustion in an internal combustion engine has been developed. It is a three-zone model, including unburned, burned, and flame front zones, in which the flame has a spherical shape and propagates with a speed that is a combination between the turbulent and the laminar flame speeds. This model was developed in MATLAB and implemented afterwards in ICES, Volvo's internal combustion engine simulation program.

The laminar flame speed was modelled taking advantage of a detailed chemical-kinetics mechanism for a hydrogen-air mixture combined with a freely propagating flame in Cantera. The model has been simulated with different equivalence ratio, temperature, pressure and dilution in order to determine the influence of each variable on the laminar flame speed. The simulation data has been stored and used as a basis to fit into the laminar flame speed equation.

The fitting has been done in two different ways. Method 1 handles each influencing variable, temperature and pressure influences, separately, while in method 2 these variables have been treated simultaneously. Method 2 was chosen since it provided acceptable and reasonable result.

Turbulence has been considered in the model by taking advantage of the turbulent kinetic energy, TKE , and turbulent intensity, TI . A routine to calculate the volume of the flame has been developed, which is used to keep track of the flame propagation as a function of time. The flame volume routine together with TKE and TI , is used to calculate the entrained mass.

The results of parameter sweeps show reasonable trends and the model represents a basis, from which future modifications and improvements are possible. The first step in the future work will be to calibrate and validate the model with the experimental data.

Bibliography

References

- [1] Hannah Ritchie, Max Roser, and Pablo Rosado. CO₂ and greenhouse gas emissions. *Our World in Data*, 2020.
- [2] Wikipedia contributors. Hydrogen internal combustion engine vehicle — Wikipedia, the free encyclopedia. https://en.wikipedia.org/w/index.php?title=Hydrogen_internal_combustion_engine_vehicle&oldid=1121885570, 2022. [Online; accessed 7-December-2022].
- [3] Alastair C. Lewis. Optimising air quality co-benefits in a hydrogen economy: a case for hydrogen-specific standards for NO_x emissions. *Environmental Science: Atmospheres*, 2021.
- [4] L.M. Das. 7 - hydrogen-fueled internal combustion engines. In Frano Barbir, Angelo Basile, and T. Nejat Veziroğlu, editors, *Compendium of Hydrogen Energy*, Woodhead Publishing Series in Energy. Woodhead Publishing, Oxford, 2016.
- [5] Sunita Sharma and Sib Krishna Ghoshal. Hydrogen the future transportation fuel: From production to applications. *Renewable and sustainable energy reviews*, 2015.
- [6] Zbigniew Stepień. A comprehensive overview of hydrogen-fueled internal combustion engines: Achievements and future challenges. *Energies*, 2021.
- [7] David E. Foster. An overview of zero-dimensional thermodynamic models for ic engine data analysis. *SAE Transactions*, 94, 1985.
- [8] Rolf Egnell. *On Zero-dimensional Modelling of Combustion and NO_x Formation in Diesel Engines*. PhD thesis, Lund Institute of Technology, 2001.
- [9] Melih Yıldız and Bilge Albayrak Çeper. Zero-dimensional single zone engine modeling of an si engine fuelled with methane and methane-hydrogen blend using single and double wiebe function: A comparative study. *International Journal of Hydrogen Energy*, 2017.
- [10] Ruixue C Li, Guoming G Zhu, and Yifan Men. A two-zone reaction-based combustion model for a spark-ignition engine. *International Journal of Engine Research*, 22(1):109–124, 2021.
- [11] Sören Krebs and Clemens Biet. Predictive model of a premixed, lean hydrogen combustion for internal combustion engines. *Transportation Engineering*, 5:100086, 2021.
- [12] Engineering ToolBox. Fuels - higher and lower calorific values. https://www.engineeringtoolbox.com/fuels-higher-calorific-values-d_169.html, 2003. [Online; accessed 29-December-2022].
- [13] Philippe Dagaut. Chapter 8 - experiments for kinetic mechanism assessment. In Tiziano Faravelli, Flavio Manenti, and Eliseo Ranzi, editors,

- Mathematical Modelling of Gas-Phase Complex Reaction Systems: Pyrolysis and Combustion*, volume 45 of *Computer Aided Chemical Engineering*, pages 445–471. Elsevier, 2019.
- [14] Cheng Tung Chong and Jo-Han Ng. Chapter 4 - combustion performance of biojet fuels. In Cheng Tung Chong and Jo-Han Ng, editors, *Biojet Fuel in Aviation Applications*, pages 175–230. Elsevier, 2021.
- [15] John B. Heywood. *Internal Combustion Engine Fundamentals*. McGRAW-HILL International Editions, 1988.
- [16] L. Teodosio, F. Bozza, D. Tufano, P. Giannattasio, E. Distaso, and R. Amirante. Impact of the laminar flame speed correlation on the results of a quasi-dimensional combustion model for spark-ignition engine. *Energy Procedia*, 148:631–638, 2018. ATI 2018 - 73rd Conference of the Italian Thermal Machines Engineering Association.
- [17] Hugo Gefors. Laminar flame speed modeling for a 1-d hydrogen combustion model. Master’s thesis, Chalmers University of Technology, Gothenburg, Sweden, 2020.
- [18] Wikipedia contributors. Turbulence kinetic energy — Wikipedia, the free encyclopedia. https://en.wikipedia.org/w/index.php?title=Turbulence_kinetic_energy&oldid=1107623344, 2022. [Online; accessed 13-December-2022].
- [19] Moshe Matalon. The turbulent burning velocity. <https://cefrc.princeton.edu/sites/g/files/toruqf1071/files/Files/2011%20Lecture%20Notes/Matalon/Lecture-15.pdf>, 2011. [Online; accessed 13-December-2022].
- [20] Gamma Technologies. Gt-suite: Engine performance application manual, 2021.
- [21] Irina Ayelen Jimenez. *Development of Combustion Indicators for Control of Multi-fuel Engines based on new Combustion Concepts*. PhD thesis, Polytechnic University of Valencia, 2022.
- [22] Mechanical San Diego Mechanism web page and Aerospace Engineering (Combustion Research). Chemical-kinetic mechanisms for combustion applications. <http://combustion.ucsd.edu>. [Online; accessed 20-February-2023].
- [23] David G. Goodwin, Harry K. Moffat, Ingmar Schoegl, Raymond L. Speth, and Bryan W. Weber. Cantera: An object-oriented software toolkit for chemical kinetics, thermodynamics, and transport processes. <https://www.cantera.org>, 2022. Version 2.6.0.
- [24] Jinlong Liu and Cosmin E. Dumitrescu. Single and double wiebe function combustion model for a heavy-duty diesel engine retrofitted to natural-gas spark-ignition. *Applied Energy*, 248:95–103, 2019.
- [25] Wikipedia contributors. Spherical cap — Wikipedia, the free encyclopedia. https://en.wikipedia.org/w/index.php?title=Spherical_cap&oldid=1107980309, 2022. [Online; accessed 16-December-2022].

- [26] Eric W Weisstein. Circle-circle intersection: From mathworld—a wolfram web resource. <https://mathworld.wolfram.com/Circle-CircleIntersection.html>. [Online; accessed 17-January-2023].
- [27] MATLAB. Radial basis neural networks. <https://se.mathworks.com/help/deeplearning/ug/radial-basis-neural-networks.html>, 2022. [Online; accessed 17-January-2023].
- [28] Wikipedia contributors. Secant method — Wikipedia, the free encyclopedia. https://en.wikipedia.org/w/index.php?title=Secant_method&oldid=1132810330, 2023. [Online; accessed 15-January-2023].
- [29] Alexander A. Konnov, Akram Mohammad, Velamati Ratna Kishore, Nam Il Kim, Chockalingam Prathap, and Sudarshan Kumar. A comprehensive review of measurements and data analysis of laminar burning velocities for various fuel+air mixtures. *Progress in Energy and Combustion Science*, 68:197–267, 2018.
- [30] Vincent Knop, Adlène Benkenida, Stéphane Jay, and Olivier Colin. Modelling of combustion and nitrogen oxide formation in hydrogen-fuelled internal combustion engines within a 3d cfd code. *International Journal of Hydrogen Energy*, 33(19):5083–5097, 2008. 2nd Asian Bio Hydrogen Symposium.
- [31] A quasi-dimensional model for the power cycle of a hydrogen-fuelled ice. *International Journal of Hydrogen Energy*, 32(15):3545–3554, 2007. International Symposium on Solar-Hydrogen-Fuel Cells 2005.
- [32] A correlation for the laminar burning velocity for use in hydrogen spark ignition engine simulation. *International Journal of Hydrogen Energy*, 36(1):957–974, 2011. 11th International Conference: "Hydrogen Materials Science Chemistry of Carbon Nanomaterials".

Appendix

```
units(length='cm', time='s', quantity='mol', act_energy='cal/mol')

ideal_gas(name='gas',
           elements="N H O C",
           species="""H2   H    O2   OH   O
                    H2O  HO2  H2O2 N2""",
           reactions='all',
           transport='Mix',
           initial_state=state(temperature=300.0, pressure=OneAtm))

#
# Species data
#

species(name='H2',
         atoms='H:2',
         thermo=(NASA([300.00, 1000.00],
                       [ 2.34433112E+00,  7.98052075E-03, -1.94781510E-05,
                        2.01572094E-08, -7.37611761E-12, -9.17935173E+02,
                        6.83010238E-01]),
                 NASA([1000.00, 5000.00],
                       [ 3.33727920E+00, -4.94024731E-05,  4.99456778E-07,
                        -1.79566394E-10,  2.00255376E-14, -9.50158922E+02,
                        -3.20502331E+00])),
         transport=gas_transport(geom='linear',
                                 diam=2.92,
                                 well_depth=38.0,
                                 polar=0.79,
                                 rot_relax=280.0),
         note='000000')

species(name='H',
         atoms='H:1',
         thermo=(NASA([300.00, 1000.00],
                       [ 2.50000000E+00,  7.05332819E-13, -1.99591964E-15,
                        2.30081632E-18, -9.27732332E-22,  2.54736599E+04,
                        -4.46682853E-01]),
                 NASA([1000.00, 5000.00],
                       [ 2.50000001E+00, -2.30842973E-11,  1.61561948E-14,
                        -4.73515235E-18,  4.98197357E-22,  2.54736599E+04,
                        -4.46682914E-01])),
         transport=gas_transport(geom='atom',
                                 diam=2.05,
                                 well_depth=145.0),
         note='000000')

species(name='O2',
         atoms='O:2',
         thermo=(NASA([300.00, 1000.00],
                       [ 3.78245636E+00, -2.99673416E-03,  9.84730201E-06,
                        -9.68129509E-09,  3.24372837E-12, -1.06394356E+03,
                        3.65767573E+00]),
                 NASA([1000.00, 5000.00],
                       [ 3.28253784E+00,  1.48308754E-03, -7.57966669E-07,
                        2.09470555E-10, -2.16717794E-14, -1.08845772E+03,
                        5.45323129E+00])),
         transport=gas_transport(geom='linear',
                                 diam=3.458,
                                 well_depth=107.4,
                                 polar=1.6,
                                 rot_relax=3.8),
         note='000000')

species(name='OH',
         atoms='H:1 O:1',
         thermo=(NASA([300.00, 1000.00],
                       [ 4.12530561E+00, -3.22544939E-03,  6.52764691E-06,
                        -5.79853643E-09,  2.06237379E-12,  3.38153812E+03,
                        -6.90432960E-01]),
                 NASA([1000.00, 5000.00],
                       [ 2.86472886E+00,  1.05650448E-03, -2.59082758E-07,
                        3.05218674E-11, -1.33195876E-15,  3.71885774E+03,
                        ])),
         transport=gas_transport(geom='linear',
                                 diam=3.458,
                                 well_depth=107.4,
                                 polar=1.6,
                                 rot_relax=3.8),
         note='000000')
```

```

                    5.70164073E+00)),
transport=gas_transport (geom='linear ',
                        diam=2.75,
                        well_depth=80.0),
note='000000')

species (name='O',
        atoms='O:1',
        thermo=(NASA([300.00, 1000.00],
                    [ 3.16826710E+00, -3.27931884E-03, 6.64306396E-06,
                      -6.12806624E-09, 2.11265971E-12, 2.91222592E+04,
                      2.05193346E+00]),
                NASA([1000.00, 5000.00],
                    [ 2.56942078E+00, -8.59741137E-05, 4.19484589E-08,
                      -1.00177799E-11, 1.22833691E-15, 2.92175791E+04,
                      4.78433864E+00])),
        transport=gas_transport (geom='atom',
                                diam=2.75,
                                well_depth=80.0),
        note='000000')

species (name='H2O',
        atoms='H:2 O:1',
        thermo=(NASA([300.00, 1000.00],
                    [ 4.19864056E+00, -2.03643410E-03, 6.52040211E-06,
                      -5.48797062E-09, 1.77197817E-12, -3.02937267E+04,
                      -8.49032208E-01]),
                NASA([1000.00, 5000.00],
                    [ 3.03399249E+00, 2.17691804E-03, -1.64072518E-07,
                      -9.70419870E-11, 1.68200992E-14, -3.00042971E+04,
                      4.96677010E+00])),
        transport=gas_transport (geom='nonlinear ',
                                diam=2.605,
                                well_depth=572.4,
                                dipole=1.844,
                                rot_relax=4.0),
        note='000000')

species (name='HO2',
        atoms='H:1 O:2',
        thermo=(NASA([300.00, 1000.00],
                    [ 4.30179801E+00, -4.74912051E-03, 2.11582891E-05,
                      -2.42763894E-08, 9.29225124E-12, 2.94808040E+02,
                      3.71666245E+00]),
                NASA([1000.00, 5000.00],
                    [ 4.01721090E+00, 2.23982013E-03, -6.33658150E-07,
                      1.14246370E-10, -1.07908535E-14, 1.11856713E+02,
                      3.78510215E+00])),
        transport=gas_transport (geom='nonlinear ',
                                diam=3.458,
                                well_depth=107.4,
                                rot_relax=1.0),
        note='000000')

species (name='H2O2',
        atoms='H:2 O:2',
        thermo=(NASA([300.00, 1000.00],
                    [ 4.27611269E+00, -5.42822417E-04, 1.67335701E-05,
                      -2.15770813E-08, 8.62454363E-12, -1.77025821E+04,
                      3.43505074E+00]),
                NASA([1000.00, 5000.00],
                    [ 4.16500285E+00, 4.90831694E-03, -1.90139225E-06,
                      3.71185986E-10, -2.87908305E-14, -1.78617877E+04,
                      2.91615662E+00])),
        transport=gas_transport (geom='nonlinear ',
                                diam=3.458,
                                well_depth=107.4,
                                rot_relax=3.8),
        note='000000')

species (name='N2',
        atoms='N:2',
        thermo=(NASA([300.00, 1000.00],
                    [ 3.29867700E+00, 1.40824040E-03, -3.96322200E-06,

```

```

                    5.64151500E-09, -2.44485400E-12, -1.02089990E+03,
                    3.95037200E+00]),
NASA([1000.00, 5000.00],
     [ 2.92664000E+00, 1.48797680E-03, -5.68476000E-07,
       1.00970380E-10, -6.75335100E-15, -9.22797700E+02,
       5.98052800E+00])),
transport=gas_transport (geom='linear',
                        diam=3.621,
                        well_depth=97.53,
                        polar=1.76,
                        rot_relax=4.0),
note='000000')

#
# Reaction data
#
# Reaction 1
reaction('H + O2 <=> OH + O', [3.520000e+16, -0.7, 17069.79])
# Reaction 2
reaction('H2 + O <=> OH + H', [5.060000e+04, 2.67, 6290.63])
# Reaction 3
reaction('H2 + OH <=> H2O + H', [1.170000e+09, 1.3, 3635.28])
# Reaction 4
reaction('H2O + O <=> 2 OH', [7.600000e+00, 3.84, 12779.64])
# Reaction 5
three_body_reaction('2 H + M <=> H2 + M', [1.300000e+18, -1.0, 0.0],
                   efficiencies='H2:2.5 H2O:12.0')
# Reaction 6
three_body_reaction('H + OH + M <=> H2O + M', [4.000000e+22, -2.0, 0.0],
                   efficiencies='H2:2.5 H2O:12.0')
# Reaction 7
three_body_reaction('2 O + M <=> O2 + M', [6.170000e+15, -0.5, 0.0],
                   efficiencies='H2:2.5 H2O:12.0')
# Reaction 8
three_body_reaction('H + O + M <=> OH + M', [4.710000e+18, -1.0, 0.0],
                   efficiencies='H2:2.5 H2O:12.0')
# Reaction 9
three_body_reaction('O + OH + M <=> HO2 + M', [8.000000e+15, 0.0, 0.0],
                   efficiencies='H2:2.5 H2O:12.0')
# Reaction 10
falloff_reaction('H + O2 (+ M) <=> HO2 (+ M)',
                 kf=[4.650000e+12, 0.44, 0.0],
                 kf0=[5.750000e+19, -1.4, 0.0],
                 efficiencies='H2:2.5 H2O:16.0',
                 falloff=Troelike(A=0.5, T3=1e-30, T1=1e+30))
# Reaction 11
reaction('HO2 + H <=> 2 OH', [7.080000e+13, 0.0, 295.0])
# Reaction 12
reaction('HO2 + H <=> H2 + O2', [1.660000e+13, 0.0, 822.9])
# Reaction 13
reaction('HO2 + H <=> H2O + O', [3.100000e+13, 0.0, 1720.84])
# Reaction 14
reaction('HO2 + O <=> OH + O2', [2.000000e+13, 0.0, 0.0])
# Reaction 15
reaction('HO2 + OH <=> H2O + O2', [2.890000e+13, 0.0, -497.13])
# Reaction 16
falloff_reaction('2 OH (+ M) <=> H2O2 (+ M)',
                 kf=[7.400000e+13, -0.37, 0.0],

```



```
kf0=[2.300000e+18, -0.9, -1701.72],  
efficiencies='H2:2.0 H2O:6.0',  
falloff=Troe(A=0.735, T3=94.0, T1=1756.0, T2=5182.0))
```

```
# Reaction 17  
reaction('2 HO2 <=> H2O2 + O2', [3.020000e+12, 0.0, 1386.23])  
  
# Reaction 18  
reaction('H2O2 + H <=> HO2 + H2', [2.300000e+13, 0.0, 7950.05])  
  
# Reaction 19  
reaction('H2O2 + H <=> H2O + OH', [1.000000e+13, 0.0, 3585.09])  
  
# Reaction 20  
reaction('H2O2 + OH <=> H2O + HO2', [7.080000e+12, 0.0, 1434.03])  
  
# Reaction 21  
reaction('H2O2 + O <=> HO2 + OH', [9.630000e+06, 2.0, 3991.4])
```